The DOI for this manuscript is doi: 10.1175/2008BAMS2487.1

THE TERRAIN-INDUCED ROTOR EXPERIMENT:
AN OVERVIEW OF THE FIELD CAMPAIGN AND SOME HIGHLIGHTS OF SPECIAL OBSERVATIONS

Vanda Grubišić[1#], James D. Doyle[2], Joachim Kuettner[3], Stephen Mobbs[4], Ronald B. Smith[5], C. David Whiteman[6], Richard Dirks[3], Stanley Czyzyk[7], Stephen A. Cohn[3], Simon Vosper[8], Martin Weissmann[9], Samuel Haimov[10], Stephan De Wekker[11], Laura L. Pan[3], Fotini Katopodes Chow[12]

[1]Desert Research Institute, Reno, NV
[2]Naval Research Laboratory, Monterey, CA
[3]National Center for Atmospheric Research, Boulder, CO
[4]University of Leeds, Leeds, UK
[5]Yale University, New Haven, CT
[6]University of Utah, Salt Lake City, UT
[7]National Weather Service, Las Vegas, NV
[8]Met Office, Exeter, UK
[9]DLR, Oberphaffenhoffen, Germany
[10]University of Wyoming, Laramie, WY
[11]University of Virginia, VA
[12]University of California, Berkeley, CA

Submitted for publication to the
Bulletin of the American Meteorological Society
August 17, 2007

Revised manuscript submitted
December 21, 2007

[#] Corresponding author address: Dr. Vanda Grubišić, Division of Atmospheric Sciences, Desert Research Institute, 2215 Raggio Parkway, Reno, NV 89512. E-mail: Vanda.Grubisic@dri.edu

ABSTRACT

The Terrain-Induced Rotor Experiment (T-REX) is a coordinated international project, comprised of an observational field campaign and a research program, focused on the investigation of atmospheric rotors and closely related phenomena in complex terrain. The T-REX field campaign took place during March and April 2006 in the lee of the southern Sierra Nevada in eastern California. Atmospheric rotors have been traditionally defined as quasi-two-dimensional atmospheric vortices that form parallel to and downwind of a mountain ridge under conditions conducive to the generation of large-amplitude mountain waves. Intermittency, high-levels of turbulence, and complex small-scale internal structure characterize rotors, which are known hazards to general aviation. The objective of the T-REX field campaign was to provide an unprecedented comprehensive set of *in situ* and remotely-sensed meteorological observations from the ground to upper troposphere-lower stratosphere (UTLS) altitudes for the documentation of the spatio-temporal characteristics and internal structure of a tightly coupled system consisting of an atmospheric rotor, terrain-induced internal gravity waves, and a complex-terrain boundary layer. In addition, T-REX had several ancillary objectives including the studies of UTLS chemical distribution in the presence of mountain waves and complex-terrain boundary layer in the absence of waves and rotors. This overview provides a background of the project including the information on its science objectives, experimental design and observational systems, along with highlights of key observations obtained during the field campaign.

1. INTRODUCTION

Atmospheric rotors are traditionally defined as intense low-level horizontal vortices that form along an axis parallel to and downstream of a mountain ridge crest in association with large-amplitude mountain waves. High-levels of turbulence characterize rotors, which are known to pose a great hazard to aviation. Recent numerical, theoretical, and observational studies of rotors (Clark et al. 2000; Doyle and Durran 2002, 2004, 2007; Vosper 2004; Hertenstein and Kuettner 2005; Mobbs et al. 2005; Grubišić and Billings 2007a; Sheridan et al. 2007) show that rotors are strongly coupled to the structure and evolution of overlying mountain waves as well as to the underlying boundary layer. Consequently, the overarching objective of the Terrain-induced Rotor Experiment (T-REX) is to study synergistic interaction and coupling between rotors, mountain waves and boundary-layer dynamics.

T-REX is the second phase of a coordinated effort to explore the structure and evolution of atmospheric rotors and associated phenomena in complex terrain. The initial, exploratory phase of this effort was the Sierra Rotors Project (SRP), which completed its field activities in March and April 2004. The T-REX Special Observation Period (SOP) took place in March and April 2006 in the lee of the southern Sierra Nevada, in the same location as the SRP two years earlier.

The core T-REX scientific objectives are focused on *improving the understanding and predictability of the coupled mountain-wave, rotor, and boundary-layer system (Grubišić et al. 2004)*. This set of objectives includes examination of: i) the role of the upstream flow properties in determining the dynamics and structure of the rotor coupled system, ii) wave-rotor dynamical interactions, iii) internal rotor structure, iv) rotor-boundary layer interactions, as well as v) upper-level gravity wave breaking and turbulence. In addition, T-REX has a set of complementary scientific objectives including: i) understanding the role of mountain waves in the stratospheric-tropospheric exchange (STE), ii) structure and evolution of the complex-terrain boundary layer in the absence of rotors, and iii) layering and phase transitions in wave clouds.

This overview is meant to provide the background of the project and information on the observational component, including observational systems, experimental design, unique aspects and challenges of the T-REX field campaign along with a brief summary of the special operations and key observations obtained during the field campaign.

2. T-REX EXPERIMENT DESIGN, INSTRUMENTATION AND REAL-TIME FORECASTING

The area chosen for T-REX research was the southern Sierra Nevada in eastern California (Fig. 1). The same location was also the site of the 1950's Sierra Wave Project that, while primarily focused on mountain waves, provided some *in situ* observations also of attendant rotors (Holmboe and Klieforth 1957; Kuettner 1959; Grubišić and Lewis 2004). The spring months of March and April were selected for the T-REX field campaign based on the climatology, which indicates that April is the month with the highest frequency of mountain wave activity in the southern Sierra Nevada. Climatologically, there is also a number of days with more quiescent synoptic conditions in these two months, in particular within the month of March (Grubišić and Billings 2007b).

2.1 Location

The Sierra Nevada is a north-northwest to south-southeast oriented mountain range of about 600 km length and 100 km width with a sharp, well-defined ridgeline. Its southern part is the tallest, quasi two-dimensional topographic barrier in the contiguous United States with a number of peaks above 4 km, including the highest peak in the 48 contiguous states (Mt. Whitney 4,418 m) and the steepest lee slopes (~30 degrees). Due to the modest height of coastal mountain ranges of California, air masses of a general westerly origin off the Pacific Ocean reach the Sierra Nevada western slopes with little deflection and minor perturbations induced by the underlying terrain. Owens Valley, located between the southern Sierra Nevada to the west and the White-Inyo mountain range (~3 km high peaks) to the east, is a north-northwest to south-southeast-oriented rift valley of 150 km length and 15-30 km width. The average elevation difference between the Sierra crest and the valley floor is about 3,000 m. Located at the southern end of Owens Valley is the largest point source of fugitive dust in the Western Hemisphere–the dry Owens Lake bed covering the area of 280 km^2. In strong wind events, up to 70 tons of dust can be blown from the lakebed per second, generating dust storms in Owens Valley in which concentrations of particulate matter 10 μm and less in diameter (PM_{10}) have reached 40,000 μg m^{-3} (Raloff 2001). The main theater of T-REX operations was located in the central portion of Owens Valley, near the town of Independence, approximately 15 km to the north of the dry Owens Lake bed.

2.2 Pilot Sierra Rotors Campaign

The goals of the pilot Sierra Rotors Project (SRP) were, in part, to obtain climatological data on the locations and frequency of occurrence of rotors in Owens Valley to aide in the experimental design of T-REX. The core instrumentation in SRP consisted of a long-term network of 16 automatic weather stations (AWS) installed by the Desert Research Institute (DRI) and two Integrated Sounding Systems (ISS) deployed in Owens Valley by the National Center for Atmospheric Research (NCAR). These were supplemented by two atmospheric sounding systems in the San Joaquin Valley upwind of the Sierra Nevada (NCAR MGAUS and a GPS system at NAS Lemoore), and an instrumented vehicle (University of Innsbruck) and a time-lapse video system (Yale) in Owens Valley (Grubišić and Billings 2007a, Jiang and Doyle 2007, Raab and Mayr 2007). The SRP dataset enabled T-REX investigators to optimize the ground-based instrumentation locations and to develop coordinated observing strategies among the various observing systems for the rotor coupled system, as well as the complementary objectives.

2.3 Types of Special Operations

To collect the data needed to address T-REX scientific objectives, two types of special operations were conducted during the field campaign:

1) Intensive Observing Periods (IOP), during which comprehensive ground-based and airborne, *in situ* and remote sensing measurements were conducted in the transition period prior to and during strongly forced conditions favoring wave and rotor formation; these conditions are associated with the passage of mid-latitude weather systems with mostly westerly synoptic-scale winds,

2) Enhanced Observing Periods (EOP) during which comprehensive observations of complex terrain boundary layer structure and evolution within Owens Valley were conducted during relatively quiescent conditions dominated by large-scale high-pressure systems.

2.4 Instrumentation

The T-REX experimental design reflects the need to document a coupled system of considerable vertical extent, reaching from the ground to the lower stratosphere. For this reason, the field campaign had both substantial ground-based and airborne components. The ground-based instrumentation was also used to document the structure and evolution of the complex-terrain boundary layer in the absence of rotors.

2.4.1 Ground-based Instrumentation

The majority of the ground-based instrumentation was deployed within the focus area in Owens Valley, extending the scope and the cross- and along-valley extent of the SRP deployment in 2004 (Fig. 2). In addition to a more extensive network of surface sensors and upper-air soundings, the ground-based remote sensing capability was also significantly expanded in T-REX. This expanded capability included two Doppler lidars, one aerosol lidar, three sodars and Radio Acoustic Sounding Systems (RASS), and three boundary-layer (915 MHz) wind profilers (of which one was mobile; all part of NCAR Integrated Sounding Systems (ISS)). The performance of the lidars benefited from the presence of dust from the dry Owens Lake bed (Fig. 1); airborne dust enhances the aerosol backscatter, which improves the overall lidar capability to measure the flow and document small-scale structures and turbulence. The flux measuring capability consisted of three 30-m flux towers (NCAR ISFF), the Outdoor Three-dimensional In-situ calibrated Hot-film anemometry System (OTIHS), and five shorter flux towers within the valley. The more extensive networks of surface sensors included additional AWS, temperature data loggers, soil temperature/moisture sensors, all supplementing the pre-existing long-term AWS network and an instrumented vehicle. Upper-air soundings were made from two GPS radiosonde launch sites in the valley near Independence. Additionally, a fixed and a mobile GPS site, a thermosonde[1], and a K-band radar were operated upwind of the Sierra Nevada to monitor the state of the incoming flow. Table 1 lists all T-REX ground-based systems. Approximately two thirds of these systems were provided by individual T-REX investigators; the remaining third was deployed and supported by the NCAR Earth Observing Laboratory (EOL).

2.4.2 Airborne Platforms and Instrumentation

To document the mesoscale structure and evolution of the wave/rotor part of the coupled system over Owens Valley, as well as the kinematic and thermodynamic structure of airflow throughout the depth of the troposphere up- and down-stream of the Sierra Nevada range, three research aircraft were involved in the T-REX campaign (Fig. 3). These were the NSF/NCAR High-performance Instrumented Airborne Platform for Environmental Research (HIAPER; Laursen et al. 2006) (120 hrs, 2 month deployment), the UK Facility for Airborne Atmospheric Measurements (FAAM) BAe146 (50 hrs, Mar 17–Apr 9 deployment), jointly operated by the Met Office and the National Environmental Research Council (NERC), and the University of Wyoming King Air (UWKA) (100 hrs, 2 month deployment). The three aircraft covered a range of altitudes from nearly 150 m above ground within Owens Valley to about 14 km MSL. The theater of airborne special operations extended from about 200 km upwind of the Sierra Nevada, over the Central Valley of California, to about 100 km downwind to the east of the Inyo Range. In addition to the probes for *in situ* kinematic and thermodynamic measurements, the special instrumentation carried by the aircraft included: i) the Wyoming Cloud Radar (WCR on board UWKA), ii) *in situ* chemical tracer instruments and microphysics probes (HIAPER and BAe146), and iii) dropsonde systems (HIAPER and BAe146) (Fig. 3).

Figure 3 also illustrates the strategy for simultaneous stacked measurements by the three aircraft and their position relative to the waves and rotors. The two jet aircraft flew an elongated racetrack pattern that was centered over Owens Valley and extended over both mountain ranges, whereas the UWKA flight pattern consisted of a single cross-mountain track, sometime supplemented with a box pattern flown within Owens Valley (Fig. 4). UWKA flew closest to

---

[1] Thermosonde is a balloon-borne instrument used to measure optical turbulence in the atmosphere.

rotors, documenting the flow structure and evolution near and below the mountain-ridge height and penetrating a number of rotors. The direction of the tracks was chosen to be nearly parallel to the wind, and was selected from among the three preset tracks: A (275 deg), B (245 deg), and C (215 deg). In addition to the coordinated multiple-aircraft coupled rotor system missions, the BAe146 aircraft flew several cold pool, cloud microphysics, and atmospheric chemistry research missions.

2.5 Operation Center and Logistics

The main T-REX Operations Center was located in Bishop, CA. The Bishop Operations Center (BOC) was located at the Owens Valley campus of the White Mountain Research Station (WMRS), a field station of the University of California. The UWKA and its support staff were located at the nearby Bishop Airport. Two satellite operations centers were set up to support HIAPER and BAe146 operations at their bases. HIAPER operated out of its home base at the NCAR/RAF facility at the Jefferson County Airport in Broomfield, CO. The BAe146 and its support staff were stationed at the Fresno International Airport (FIA), on the west side of the Sierra Nevada. The weather forecasting support was provided by the NWS Las Vegas Forecast Office throughout the field season. They brought valuable experience and local knowledge to the project planning process. The Daily Planning Meetings involved interactive audio/video connections between the BOC, RAF, FIA, NWS Las Vegas, and a number of auxiliary sites. Interactive communications were carried out using AccessGrid and other teleconferencing systems. The NCAR Field Project Support (FPS) provided logistical and operational support for the BOC including coordination of the ground-based and airborne operations as well as support of the T-REX Field Catalog (http://catalog.eol.ucar.edu/trex/). A special tool set was developed within the Interactive Data Viewer (IDV) by UCAR's Unidata program to allow interactive 3-D displays combining data from various T-REX observational platforms and model sources to aid in coordinating operations and examining data in near-real time. Figure 4 shows an IDV display of flight tracks of the three aircraft during a coordinated three-aircraft mission in IOP 6 on 25 Mar 2006.

2.6 Real-Time Forecasting

The field operations were supported by a real-time forecasting effort that included a number of mesoscale, large-scale medium-range, and mountain-wave prediction models. The special real-time models and outputs provided in support of T-REX were augmented by the widely available forecast models from the U.S. and international operational weather centers. High-resolution mesoscale forecast models were executed by a number of groups in support of the T-REX forecasting operations. These models are summarized in Table 2 and include the Coupled Ocean/Atmosphere Mesoscale Prediction System (COAMPS), the Weather Research and Forecasting Non-hydrostatic Mesoscale Model (WRF-NMM) and Advanced Research WRF (WRF-ARW), and the Fifth-generation Penn State/NCAR Mesoscale Model (MM5). Because of timeliness and availability issues, the T-REX forecasters primarily relied on the 2-km resolution COAMPS, 4-km resolution WRF-NMM, and the NCEP North American Mesoscale Model (NAM) for mesoscale model guidance. The real-time models were of insufficient horizontal resolution to predict the occurrence of rotors. However, the models were able to successfully predict the occurrence of mountain waves and their basic characteristics including the dominant wavelength and amplitude, which are hypothesized to be linked to boundary-layer separation and rotor development. An example of a real-time type of forecast product from COAMPS is shown in Fig. 5 for IOP 6. The 30-h forecast shows a series of strong lee waves downstream from the Sierra crest, which was generally confirmed by the aircraft observations. Diagnostic fields from the European Center for Medium Range Forecasts (ECMWF) Integrated Forecasting System (IFS) were computed by DLR and communicated to the BOC daily, which enabled reasonably accurate medium range forecasts of mountain wave events to be achieved. Other medium-range models that were used for real-time forecasting included NCEP GFS, the Met Office Unified Model, and the Navy NOGAPS. Linear non-hydrostatic model forecasts for the T-REX region were performed by the Met Office and NRL-Monterey groups. Although these models are rather simple in formulation relative to the more complex research and operational non-hydrostatic prediction systems, the linear tools provided useful short-term and medium-range guidance for T-REX mission planning.

3. UNIQUE AND CHALLENGING ASPECTS

As with any field campaign, there were unique aspects and challenges, some of which we mention here.

- T-REX was the first operational field project deployment for the new NSF/NCAR HIAPER aircraft. HIAPER "commuted" to Owens Valley from its home base at the NCAR/RAF facility at the Rocky Mountain Metropolitan Airport in Broomfield, Colorado. The approximately 3,000 km round-trip commute took little over four hours for this Gulfstream V jet aircraft with valuable data in the UTLS region collected en route. Due to its long endurance, HIAPER was able to spend on average close to five hours within the target area in the Sierra Nevada, before having to embark on return.

- T-REX was the first field campaign to use an airborne Doppler radar (Wyoming Cloud Radar) to obtain detailed airflow measurements within atmospheric rotors. This was also the first mountain meteorology field campaign to have had two ground-based Doppler lidars, creating an opportunity for the first-ever dual Doppler analyses of terrain-induced flows. Another unique aspect of the field campaign was the flexibility to reconfigure the wind profiler network from an across-valley to an L-shaped configuration.

- T-REX aircraft were based at three different locations, creating a need for multiple operation centers. The AccessGrid (AG) technology was used successfully for the first time in support of a complex atmospheric science field campaign to connect multiple operation centers (BOC, FIA, NCAR/RAF), and to entrain investigators from other off-site locations (DRI, other NCAR sites). Despite a fairly low-bandwidth available at BOC, the AG provided a critical communications link to overcome some of the challenges arising from the distributed nature of the T-REX operations.

- T-REX project domain included military restricted airspace and some of the most tightly protected wilderness areas on the ground. Cooperation between the T-REX staff and the military and federal agencies made it possible for T-REX aircraft to complete a number of successful coordinated missions and release a large number of dropsondes.

4. T-REX SPECIAL OPERATIONS AND HIGHLIGHTS OF PRELIMINARY FINDINGS

4.1 Overview of Special Operations

Spring 2006 was a very active mountain wave season. A large number of mid-latitude weather systems–significantly larger than is the climatological average, especially in March–passed over the T-REX project area, creating many opportunities for special observations of the rotor coupled system. Periods of quiet weather optimal for boundary-layer studies were short, increasing in number and length only in the second half of April. The springtime 2006 period also featured significant precipitation in the Sierra Nevada, bringing the effect of moisture on mountain waves and rotors more strongly into our focus.

Fifteen IOPs were conducted during the two-month field campaign. The IOPs ranged in length from 4 to 39 hours, with the average length of about 24 hours. The majority of IOPs covered both transitions toward as well as the periods of strongest wave/rotor activity. All available ground-based and airborne instrumentation platforms were used in IOPs. The radisonde launches, both upstream and downstream of the Sierra Nevada, were carried out every three hours. The total number of research flights flown during the field campaign was twelve by HIAPER and BAe146 each, and twenty-five by UWKA. These flights were flown in IOPs with the exception of several BAe146 research flights and the aircraft intercomparison mission on 6 Apr 2006 flown by all three aircraft. The majority of IOP flights were part of coordinated aircraft missions involving two (HIAPER and UWKA or BAe146 and UWKA) or all three aircraft. The average research mission length was 8.8 hrs for HIAPER, 4.5 hrs for BAe146, and 3.5 hrs for UWKA. Table 3 presents the summary of T-REX IOPs, the research aircraft flights flown in them, and the number of dropsondes and radiosondes.

In addition, five EOPs were carried out (Table 4) to observe the normal diurnal evolution of the valley boundary layer under undisturbed conditions. EOPs were fixed-length observing periods starting in the early afternoon (at 2300 UTC) of day one and ending at noon (2000 UTC) the next day. While centered on nighttime, they covered a nearly full 24-hour period, including the morning and evening transition periods when the atmosphere was most rapidly changing. Special observations during these periods included radiosonde launches at 3-hour and 1.5-hour intervals from the Independence Airport site, lidars, and BAe146 supporting flights in Owens Valley, supplementing other continuous ground-based measurements in the valley.

4.2 Highlights of Preliminary Findings

4.2.1 Coupled Mountain Wave/Rotor/Boundary-Layer System

The T-REX observational data provide an unprecedented coverage of the rotor phenomenon and its dynamical linkages with the overlying mountain-wave and the underlying boundary-layer evolution and structure. Several rotor events were successfully documented during the experiment. A number of these rotor events also exhibited transitions from weakly perturbed conditions characterized by the presence of small to moderate amplitude mountain waves above the Sierra ridge to strongly perturbed conditions with large-amplitude waves above and within Owens Valley, favoring rotor formation. The combination of *in situ* measurements by the aircraft and remotely-sensed measurements by airborne WCR as well as ground-based lidars, wind profilers and surface stations offers a unique opportunity to study: (i) the wave-rotor dynamical interactions, (ii) the internal rotor structure, and (iii) the rotor-boundary layer interactions.

An example of the coupling between mountain waves and a rotor is illustrated in Fig. 6, which displays vertical velocity measured by the three T-REX aircraft in a range of altitudes from about 2 km to 14 km MSL on 25 Mar 2006 during a coordinated three-aircraft mission in IOP 6. The data shown in this figure was collected over several hours. Large-amplitude waves were present at all levels, but there is a clear contrast between smooth wave motions above ~7 km MSL and increasing amounts of turbulence below this altitude. The amplitude of the wave motions, as well as turbulence, were at a maximum below the Sierra ridge, where the UWKA measured positive and negative vertical velocities in excess of 15 and -10 m s^{-1}, respectively, along the northern face of the box pattern (not shown). While the wave field in Fig. 6 appears fairly steady, especially below 7 km MSL, as indicated by little change in wave amplitude and phase between repeated legs by BAe146 and UWKA, even at those altitudes the waves were not steady at all times during this IOP. The time-height plots of vertical velocity from a network of three boundary-layer wind profilers in Fig. 7 illustrates the low-level waves and their unsteadiness for a 12-hr period during the early morning hours on 25 Mar preceding the aircraft flights. This diagram shows the vertical velocity above the West (ISS), Center (MISS), and East (MAPR) wind profiler sites, arranged along a cross-valley transect passing just south of Independence. The horizontal separation between the profilers was approximately 5 km. Persistent upward- or downward-directed vertical motion above the wind profiler is consistent with a lee wave overhead. The strength and even sign of the motion above the profiler depends on the phase of the wave and its amplitude. Areas of blue are updrafts that persisted over time and height, while yellow and red show persistent downdrafts. At each site, the wave was seen to change significantly over time, with phase changes between updraft and downdraft (for example near 1000 UTC 25 Mar in the West and Center sites and 1100 UTC 25 Mar at the East site), and changes in downward penetration of the wave into the valley. The wind profiler network also reveals how the wave pattern changed across the valley. For example, at 0830 UTC at 4.3 km MSL (blue vertical lines and circles), the West profiler shows a downdraft while the Center and East profilers show updrafts. Similarly, the red lines and the circle are for measurements at 1300 UTC 25 Mar, when the West profiler shows an updraft and the Center and East profilers observe downdrafts. It is rare – perhaps unique – to have a cross section of wave observations with continuous coverage in height and time; this is only possible with a network such as was deployed in T-REX. A more in-depth analysis of this data, in conjunction with the analysis of upstream and in-valley soundings and lidar data, can be used to examine the changing structure of the wave over time and height and to address another of the T-REX objectives, namely, the role of the upstream flow properties in determining the evolution and structure of the rotor coupled system.

During the two days of IOP 6 (20 UTC 24 Mar – 20 UTC 26 Mar) a number of different wave responses over the valley and types of flow within the valley were observed, pointing toward a complex interaction between waves and the boundary layer within this deep and wide valley.

During the morning and mid-day hours of 25 Mar, trapped lee waves with a lee-wave rotor, characterized the flow over Owens Valley (consistent with clouds shown in Fig. 8). Later, a cold frontal passage changed the upstream conditions significantly, leading to the development in the afternoon hours of a severe downslope windstorm. This was the strongest windstorm of the T-REX period, with maximum wind gusts in the valley of 31.7 m s^{-1} recorded by DRI tower 2 at the west end of the valley. Figure 9 shows the zonal and meridional components of surface wind in the valley measured during IOP 6 by the northernmost of the tree cross-valley transects of DRI AWS network. The strongest surface signatures, characterized by alternating periods of westerly and easterly flow, are found during the twelve-hour period from 1600 UTC 25 Mar to 0400 UTC 26 Mar. The flow within the valley was, however, highly three-dimensional as indicated by a strong meridional wind component, which shows equally complex variability over time and space. The most striking feature during this period is certainly a southwesterly windstorm that swept across Owens Valley soon after 0200 UTC 26 Mar. The cross-valley extent of this flow changed significantly with time; between 0200 UTC and 0400 UTC it retreated westward and was replaced by, at times, equally strong N-NE down-valley flow. Strong pressure gradients (up to 5 hPa over 10 km) at the ground, as well as observations of the flow over the valley by the Doppler and aerosol lidars and wind profilers during this period, suggest a resemblance of this flow feature to a propagating hydraulic jump. Figure 10 shows the DLR Doppler lidar observations at the time when this feature had already retreated to the west of the DLR lidar site on the alluvial slope at the west side of the valley. The lidar plan position indicator (PPI; horizontal) scan (Fig. 10a) shows strong westerly and south-westerly winds to the west of the lidar site, and weaker northerly, along-valley winds to the east of the windstorm front or the jump location. Evident are also several streaks in the downslope flow and a curvature of the interface between the strong W or SW winds and the weaker northerly flow that is deflected eastwards. Significant temporal variability of lidar scans during this time, evident in animation loops, indicates that this flow was extremely turbulent and transient.

High-resolution scans by the REAL aerosol lidar provide an unprecedented visualization of flow structures within and above boundary layer as revealed by inhomogeneities in the aerosol distribution. Figure 11 shows a range height indicator (RHI; vertical) scan from REAL obtained during IOP 1 on 3 Mar 2006. This scan was completed in about 30 sec. The air that flows down the east side of the Sierra slopes (indicated by the white arrow near the surface from left to right) is relatively clean and undercuts the aerosol-laden air in Owens Valley. Aerosol-laden air from Owens Valley, which has an easterly flow component (indicated by the white arrow near the surface from right to left), converges with the westerly flow down the Sierra slopes. The resulting convergence zone is visible as are the resulting circulations with aerosols transported upwards and then horizontally and downward at higher elevations (indicated by the black arrows). The image and the animation suggest there are two counter-rotating circulations with two separate horizontal axes that are aligned in the north-south direction along the Sierra range. The circulation on the eastern (right) side of the convergence area may indicate the presence of a rotor-like system given simultaneous UWKA observations of waves and an elevated turbulent zone. The REAL and Doppler lidar observations often indicated the presence of coherent small-scale structures embedded within the shear layer at the leading edge of the lee waves, consistent with expectations based on numerical modeling studies (e.g., Hertenstein and Kuettner 2005; Doyle and Durran 2007).

Observations by the airborne Doppler WCR, in conjunction with *in situ* measurements by UWKA and observations by REAL and the two ground-based Doppler lidars, offer the opportunity to reveal spatial and temporal scales of motions in the interior of a rotor. Figure 12 shows an example of a dual-Doppler synthesis of the flow field within a rotor cloud over Owens Valley from IOP 11 (at 2310 UTC 9 Apr 2006) obtained using the technique described in Damiani and Haimov (2006). In this event, the rotor cloud over the valley, whose depth at the time of this pass ranged from 2.3 to 2.9 km, extending approximately between flight levels at 3.7 and 6.4 km MSL, had a rather ragged western edge, yet the flow through the top portion of that cloud was surprisingly smooth as revealed by the streamlines shown in black.

During IOPs, many upstream radiosonde launches from the southern San Joaquin Valley, immediately west of the Sierra Nevada, were accompanied by simultaneous launches from Owens Valley. There are 102 such sounding pairs available from the two-month field campaign, which contain a wealth of information on the influence of a mountain range on the atmosphere. Figure 13 compares the wind speed and relative humidity at 500 and 700 hPa pressure levels on both sides of the Sierra Nevada. At 500 hPa, above the Sierra crest, the wind data falls close to the 1-to-1 line with as many points below as above this line, indicating that the mountain range produces little disturbance to the synoptic wind fields at this level. At 700 hPa, below the crest level, winds are substantially reduced on the east, the lee side of the Sierra. The terrain-induced effects are also clearly shown in relative humidity differences between the two sides, with a substantial drying at 700-hPa pressure level on the lee side of the Sierra Nevada.

Another ensemble view of the data is presented in Fig. 14, which shows the relationship between energy and momentum fluxes for mountain waves in the upper troposphere-lower stratosphere. The data used in this analysis was obtained by HIAPER in the approximate range of altitudes from 9 to 14 km during six Track B large-amplitude mountain wave flights. The availability of the GPS altitude data has made the direct computation of wave energy flux possible for the first time using the aircraft ambient pressure measurement. The data in Fig. 14 shows that the relationship between energy and momentum fluxes predicted by Eliassen and Palm (1961) for steady small-amplitude non-dissipative mountain waves holds also for these large-amplitude waves generated by the Sierra Nevada and even extends to the region of negative energy and positive momentum fluxes. A detailed discussion of this analysis and the physical reasons for the latter can be found in Smith et al. (2007).

4.2.2 Role of mountain waves in the UTLS chemical distribution

In addition to the meteorological parameters, a small suite of chemical tracers, including ozone (O_3), carbon monoxide (CO) and water vapor (H_2O), were measured onboard HIAPER during the T-REX missions.[2] The variation and correlation of these tracers provide a unique perspective as to how the air mass is affected by waves and whether mixing has occurred in the UTLS region. In particular, O_3 and CO are frequently used as tracers in stratosphere-troposphere exchange (STE) studies (e.g., Fischer et al. 2000; Zahn et al. 2000; Hoor et al. 2002; Pan et al. 2004). O_3 increases rapidly above the tropopause and is often used as a tracer for stratospheric air. CO, on the other hand, decreases rapidly above the tropopause and is used as a tracer for the

[2] The ozone measurements were made with the NCAR Ozone Chemiluminescence instrument; the CO measurements were made with a VUV resonance fluorescence instrument; and the water vapor was measured with a MayComm Open-Path Laser Hygrometer (OPLH) sensor. All three instruments provided data at ~1 second sampling rate.

tropospheric air. The mixing ratios of both tracers go through steep gradients in the tropopause region, which helps identify the chemical transition from stratosphere to troposphere. The correlation between the two tracers often highlights the mixing between the stratospheric and tropospheric air masses.

A striking case of mountain wave perturbation to the lower stratospheric chemical distribution was observed during HIAPER flight on 15 Apr 2006 (IOP 13) after the aircraft exited the racetrack pattern within the T-REX target area over the Sierra Nevada and Owens Valley. As HIAPER ascended to approximately 14.5 km over the mountain ranges of central Nevada large amplitude waves appeared in the ozone signal. A series of mountain waves was seen in the ozone data with large amplitudes exceeding 300 ppbv in ozone mixing ratio, representing a factor of 2 or more increase in flight-level ozone values. Figure 15 shows the O_3 and CO time series for a 7-min segment of this flight together with the time series of potential temperature and vertical velocity. The mountain wave signature in the CO time series is anti-correlated with O_3, whereas the potential temperature and vertical velocity display phase shift characteristic for internal gravity waves. The O_3 and CO also form a compact relationship in the tracer space (not shown).

4.2.3 Structure and evolution of the complex-terrain boundary layer under quiescent conditions

Overall, observations from the EOPs indicated the presence of thermally-driven valley wind systems acting under the influence of synoptic conditions and local forcing due to the topography and geographic location of Owens Valley. At the valley surface, the flow usually transitioned from up-valley during the day, to down-valley at night, as expected under quiescent conditions. Morning transitions back to up-valley flow were also observed. Analysis of vertical wind profiles in Owens Valley, however, revealed a much more complex wind structure.

Particularly interesting was the development of the nocturnal boundary layer observed during EOP 2 (30 Mar 2006), which illustrates the combined influence of synoptic and local forcing. Despite strong winds above ridge tops (see Table 4), EOP 2 exhibited relatively quiescent conditions in the valley. Rawinsonde profiles from Independence Airport (Fig. 16a) reveal the development of a three-layer flow structure beginning in the late evening hours (local time) of 29

March. This three-layer structure consisted of a stably-stratified down-valley flow near the surface and an elevated up-valley flow in the near-neutral residual layer, both entirely decoupled from the westerly flow above the tops of the surrounding mountains. Flow above the ridge crests was westerly or northwesterly throughout EOP 2, and was separated from the valley atmosphere by a strong inversion. The flow structure within the valley resulted from the presence of mid-level pressure gradient opposing the low-level thermal forcing. The down-valley flow at the surface had a magnitude of 5-10 m s^{-1} and was initially coupled with an up-valley flow of weaker magnitude, which occurred between 2600 and 3400 m MSL. The up-valley flow grew and the down-valley surface wind weakened during the night, with elevated up-valley flow of magnitude 5-10 m s^{-1} occurring between 2000 and 3300 m MSL just before sunrise. The capping inversion subsided during the night, with the valley boundary layer depth decreasing from ridge crest height (~4200 m) to 3300 m MSL by sunrise. Within an hour or two after sunrise, the down-valley flow disappeared entirely, and up-valley flow was observed over the whole boundary layer depth. This flow pattern is confirmed by preliminary analysis of the Doppler lidar data as well, which indicates three distinct layers and flow directions in the valley atmosphere (Fig. 16b). The strong agreement between rawinsonde and lidar observations gives strong credence to this rarely observed three-layer flow structure, discussed in more detail in Schmidli et al. (2007).

5. SUMMARY AND OUTLOOK

The synthesis of observations from novel observing systems with routine measurements and advanced modeling activities constitutes a general aim of the T-REX research program, which is well underway. The observational highlights presented here illustrate only a small portion of what was observed during the T-REX field campaign. The forthcoming T-REX research papers are expected to describe in detail flow structures found from the ground to the UTLS region. One set of conclusions, however, has already emerged---the flow in the lee of the Sierra Nevada, both within and above Owens Valley and under strongly forced as well as more quiescent conditions, is complex, strongly nonlinear, with pronounced three-dimensional characteristics, and overall fairly sensitive to changes in upstream conditions. In addition to rotors events, which were expected to be strongly turbulent near and below the Sierra crest, strong turbulence associated with pronounced directional wind shear was found in a number of wave events in which the flow and waves above the mountain crests were found to be decoupled from the valley flow. Measurements by the airborne and ground-based remote sensors suggest that the rotors contain coherent small-scale flow structures that are embedded within the larger-scale circulations. The surface wind in the valley during wave and rotors events was often characterized by strong flow channeling but it had also displayed high degree of spatial variation, including flow reversals and convergences. Given that the characteristics of mountain waves, the timing and appearance of rotor events, and the characteristics of valley flows varied considerably from case to case, the comprehensiveness of the T-REX data set and the vast amount of data it contains represent great assets to the observational analysis effort.

These data sets will allow for some of the first comprehensive studies of the interior of elevated turbulent zones in the lee of complex terrain, characterization of turbulence, and the tight coupling between the terrain-induced waves and boundary-layer dynamics. A particularly exciting aspect of that research effort is the integration of observations from multiple surface sensors, ground-based remote sensors, and upper air and airborne measurements to produce a more complete picture of the spatial and temporal characteristics of flows above and within Owens Valley during the wave and rotor events as well as the structure of the valley boundary-layer under more quiescent conditions.

Teams of international investigators will likely use T-REX data for years to come. The T-REX data set will also be extremely valuable for evaluation of numerical models in a challenging complex-terrain environment and will provide future opportunities for testing new data assimilation strategies from the mesoscale to the microscale.

ACKNOWLEDGMENTS

T-REX could not have been carried out without the dedication and vital assistance of a large number of people. T-REX investigators and participants come from a large number of US universities and agencies, the National Center for Atmospheric Research (NCAR), and several European universities and research institutes. The outstanding efforts of the T-REX field campaign participants, including the NCAR Field Project Support (FPS), and the T-REX staff are greatly appreciated. The primary sponsor of T-REX is the

US National Science Foundation (NSF), whose support is gratefully acknowledged. We acknowledge also other funding agencies and organizations that have provided funding and in-kind support for various T-REX components including the UK Natural Environmental Research Council (NERC), Met Office UK, US Naval Research Laboratory (NRL), Air Force Research Laboratory (AFRL), National Oceanic and Atmospheric Administration (NOAA), Deutsches Zentrum für Luft- und Raumfahrt (DLR), Swiss National Science Foundation (SNSF), and the Austrian Science Foundation (FWF). We thank the staff of the White Mountain Research Station for their hospitality and logistics support of the Bishop Operations Center (BOC). We would especially like to acknowledge the extraordinary support by the NWS Las Vegas Forecast Office staff in providing daily forecasts of weather conditions suitable for T-REX objectives, and Brian Billings of DRI for his dedicated nowcasting support of aircraft operations at BOC. We also thank the staff of NAS Lemoore for launching GPS radiosondes in support of our operations, and the Complex Control Board and staff of the R–2508 Complex for assuring smooth operation of the T-REX aircraft within this complex. The superintendents of Sequoia, Kings Canyon and Death Valley National Parks, the managers of the BLM and USFS field offices in Bishop as well as of LAWPD, and the Inyo County supervisors are thanked for providing permits and their support for the T-REX field operations. Acknowledged also are efforts of Don Murray and Jeff McWhirter of Unidata in developing special IDV features for support of T-REX operations, and their help in creating Figure 5. Al Cooper from NCAR is thanked for his help with many aspects of the HIAPER operation, and in particular for his supporting role as the dropsonde scientist on the majority of T-REX HIAPER flights. We thank Jim Moore for his enthusiastic and dedicated support of coordinated aircraft operations, and the valuable comments he provided for this paper. We would also like to acknowledge contributions of many people from the MetOffice, UK in particular those of Peter Sheridan and Phil Brown. The first author's research and field participation was supported by NSF grant ATM–0524891 to DRI. The second author was supported by ONR PE–0601153N. NCAR is funded by the National Science Foundation.

APPENDIX A: DATA ACCESS AND ARCHIVES

The field catalog with daily reports and quick-look data displays from all T-REX missions and operations is available at http://catalog.eol.ucar.edu/trex/. The final quality controlled data sets are available from the T-REX Data Archive, accessible from the main T-REX web pages at http://www.eol.ucar.edu/projects/trex/. The Data Archive was built and is maintained by NCAR EOL.

APPENDIX B: LIST OF ACRONYMS AND ABBREVIATIONS

3dVOM	3-D Velocities over Mountains
AFRL	Air Force Research Laboratory
AG	Access Grid
ARW	Advanced Research WRF
ASU	Arizona State University
AWS	Automatic Weather Station
BLM	Bureau of Land Management
BOC	Bishop Operations Center
COAMPS	Coupled Ocean-Atmosphere Modeling Prediction System
CTI	Coherent Technologies, Inc.
DRI	Desert Research Institute
DLR	Deutsches Zentrum für Luft- und Raumfahrt
DTC	Developmental Testbed Center (WRF)
ECMWF	European Centre for Medium-Range Weather Forecasts
EOL	Earth Observing Laboratory (NCAR)
EOP	Enhanced Observing Period
FAAM	Facility for Airborne Atmospheric Measurement (UK)
FIA	Fresno International Airport
FPS	Field Project Support (NCAR EOL)
FWF	Fonds zur Förderung der wissenschaftlichen Forschung (Austria)
GAUS	GPS Advanced Upper-air Sounding System
GFS	Global Forecast System (NCEP)
GPS	Global Positioning System
GTS	Global Transmission System
HIAPER	High-performance Instrumented Airborne Platform for Environmental Research
IDV	Interactive Data Viewer (UCAR Unidata)
IFS	Integrated Forecasting System (ECMWF)
IOP	Intensive Observing Period
ISFF	Integrated Surface Flux Facility
ISS	Integrated Sounding System
LAWPD	Los Angeles Water and Power Department
MAPR	Multiple Antennae Profiling Radar
MGAUS	Mobile GAUS

MISS	Mobile Integrated Sounding System (ISS)
MM5	Fifth-generation Penn State/NCAR Mesoscale Model
NAM	NCEP North American Mesoscale Model (former Eta)
NAS	Naval Air Station
NCAR	National Center for Atmospheric Research
NCEP	National Center for Environmental Prediction
NERC	Natural Environmental Research Council (UK)
NMM	Non-hydrostatic Mesoscale Model (WRF)
NOAA	National Oceanic and Atmospheric Administration
NRL	Naval Research Laboratory
NSF	National Science Foundation (US)
NWS	National Weather Service (US)
ONR	Office of Naval Research (US)
OTIHS	Outdoor Three-dimensional In-situ calibrated Hot-film anemometry System
PPI	Plan Position Indicator (lidar scan)
RAF	Research Aviation Facility (NCAR EOL)
RASS	Radio Acoustic Sounding System
REAL	Raman-shifted Eye-safe Aerosol Lidar
RHI	Range Height Indicator (lidar scan)
SOP	Special Observing Period
SRP	Sierra Rotors Project
STE	Stratosphere-Troposphere Exchange
T-REX	Terrain-induced Rotor Experiment
UCAR	University Corporation for Atmospheric Research
USFS	US Forest Service
UTLS	Upper Troposphere/Lower Stratosphere
UWKA	University of Wyoming King Air
WCR	Wyoming Cloud Radar
WMRS	White Mountain Research Station
WOW	Weatherstation on Wheels
WRF	Weather Research and Forecasting model

REFERENCES

Clark, T. L., W. D. Hall, R. M. Kerr, D. Middleton, L. Radke, F. M. Ralph, P. J. Nieman, and D. Levinson, 2000: Origins of aircraft-damaging clear-air turbulence during the 9 December 1992 Colorado downslope windstorm: Numerical simulations and comparison with observations. *J. Atmos. Sci.*, **57**, 1105–1131.

Cohn, S. A., W. O. J. Brown, C. L. Martin, M. S. Susedik, G. Maclean, and D. B. Parsons, 2001: Clear air boundary layer spaced antenna wind measurements with the Multiple Antenna Profiler (MAPR), *Annales Geophysicae*, **19**, 845–854.

Damiani, R., and S. Haimov, 2006: A high-resolution dual-Doppler technique for fixed multi-antenna airborne radar. IEEE Trans. *Geosci. Remote Sensing*, **(42) 12**, 3475–3489.

Doyle, J. D., and D. R. Durran, 2002: The dynamics of mountain-wave induced rotors. *J. Atmos. Sci.*, **59**, 186–201.

Doyle, J. D., and D. R. Durran, 2004: Recent developments in the theory of atmospheric rotors. *Bull. Amer. Meteor. Soc.*, **85**, 337–342.

Doyle, J. D., and D. R. Durran, 2007: Rotor and sub-rotor dynamics in the lee of three-dimensional terrain. *J. Atmos. Sci.,* **64**, 4202–4221.

Fischer, H., F. G. Wienhold, P. Hoor, O. Bujok, C. Schiller, P. Siegmund, M. Ambaum, H. A. Scheeren, and J. Lelieveld, 2000: Tracer correlations in the northern high latitude lowermost stratosphere: Influence of cross-tropopause mass exchange, *Geophys. Res. Lett.,* **27**, 97–100.

Grubišić, V., and J. M. Lewis, 2004: Sierra Wave Project revisited: 50 years later. *Bull. Amer. Meteor. Soc.*, **85**, 1127–1142.

Grubišić, V., J. D. Doyle, J. Kuettner, G. S. Poulos, and C. D. Whiteman, 2004: Terrain-induced Rotor Experiment. Scientific Overview Document and Experiment Design. 72 pp. Available at http://www.eol.ucar.edu/projects/trex/.

Grubišić, V. and M. Xiao, 2006: Climatology of westerly wind events in the lee of the Sierra Nevada. *AMS 12th Mountain Meteorology Conference*, Amer. Meteor. Soc., http://ams.confex.com/ams/pdfpapers/114755.pdf

Grubišić, V. and B. J. Billings, 2007a: The intense lee-wave rotor event of Sierra Rotors IOP 8. *J. Atmos. Sci.*, **64**, 4178–4201.

Grubišić, V. and B. J. Billings, 2007b: Climatology of the Sierra Nevada mountain wave events. *Mon. Wea. Rev.*, In press.

Hertenstein, R. F., and J. P. Kuettner, 2005: Rotor types associated with steep lee topography: Influence of the wind profile. *Tellus A*, **57**, 117–135.

Holmboe, J. R., and H. Klieforth, 1957: Investigation of mountain lee waves and the airflow over the Sierra Nevada. Final Report. Department of Meteorology, UCLA, Contract AF 19(604)-728, 283 pp.

Hoor, P., H. Fischer, L. Lange, J. Lelieveld, and D. Brunner, 2002: Seasonal variations of a mixing layer in the lowermost stratosphere as identified by the CO-O3 correlation from in situ measurements, *J. Geophys. Res.*, **107(D5),** 4044, doi:10.1029/2000JD000289.

Jiang, Q., and J. D. Doyle, 2007: Diurnal variation of downslope winds in Owens Valley during the Sierra Rotors Experiment. *Mon. Wea. Rev.,* Submitted.

Kuettner, J. P., 1959: The rotor flow in the lee of mountains. GRD Research Notes, No. 6, AFCRC--TN--58--626, ASTIA Document No. AD–208862, pp.~20.

Laursen, K., D. J. Jorgensen, G. P. Brasseur, S. L. Ustin, and J. R. Huning, 2006: HIAPER: The next generation NSF/NCAR Research Aircraft. *Bull. Amer. Meteor. Soc.,* **87**, 896–909.

Ludlam, F. H., and R. S. Scorer, 1958: *Cloud study: a pictorial guide.* Macmillan, New York, 80 pp.

Mayor, S. D., and S. M. Spuler, 2004: Raman-shifted eye-safe aerosol lidar, *Appl. Optics*, **43**, 3915-3924.

Mobbs, S. D., S. B. Vosper, P. F. Sheridan, R. Cardoso, R. R. Burton, S. J. Arnold, M. K. Hill, V. Horlacher, and A. M. Gadian, 2005: Observations of downslope winds and rotors in the Falkland Islands. *Quart. J. Roy. Meteor. Soc.,* **131**, 329–352.

Pan, L. L., W. J. Randel, B. L. Gary, M. J. Mahoney, and E. J. Hintsa, 2004: Definitions and sharpness of the extratropical tropopause: A trace gas perspective, *J. Geophys. Res.,* **109**, D23103, doi:10.1029/2004JD004982.

Parsons, D. B., and Co-authors, 1994: The Integrated Sounding System – Description and preliminary observations from TOGA-COARE, *Bull, Amer. Meteor. Soc.,* **75**, 553–567.

Raab, T., and G. Mayr, 2007: Tracking the footprints of Sierra Nevada windstorms with an automobile measurement system. *J. Appl. Meteor.,* Submitted.

Raloff, J., 2001: Dust, Part 2: Ill winds. *Science News*, **160**, no. 14, 218.

Schmidli, J., G. S. Poulos, F. K. Chow, and M. H. Daniels, 2007: External influences on thermally driven flows in a deep valley. *J. Appl. Meteor.,* Submitted.

Sheridan, P. F., V. Horlacher, G. G. Rooney, P. Hignett, S. D. Mobbs, and S. B. Vosper, 2007: Influence of lee waves on the near-surface flow downwind of the Pennines. *Quart. J. Roy. Meteor. Soc.,* **133**, 1353–1369.

Smith, R. B., B. K. Woods, J. Jensen, W. A. Cooper, J. D. Doyle, Q. Jiang, and V. Grubišić, 2007: Mountain waves entering the stratosphere. *J. Atmos. Sci.,* In press.

Spuler, S. M., and S. D. Mayor, 2005: Scanning eye-safe elastic backscatter lidar at 1.54 microns, *J. Atmos. Ocean. Technol.*, **22**, 696-703.

Vosper, S. B., 2004: Inversion effects on mountain lee waves. *Quart. J. Roy. Meteor. Soc.,* **130**, 1723–1748.

Zahn, A., et al., 2000: Identification of extratropical two-way troposphere-stratosphere mixing based on CARIBIC measurements of O3, CO, and ultrafine particles*, J. Geophys. Res.,* **105**, 1527–1535.

LIST OF TABLES

LIST OF FIGURES

Figure 4: Unidata Integrated Data Viewer (IDV) display of aircraft tracks in the three-aircraft coordinated mission of T-REX IOP 6 on 25 Mar 2006.

Figure 5: Vertical velocity (color scale, increment 0.5 m s^{-1}) and potential temperature (contours interval 6 K) from a real-time 30-h COAMPS forecast for the innermost grid mesh (Δx=2 km) valid at 2100 UTC 25 Mar 2006 during IOP 6. The cross section is constructed through Independence along the HIAPER, BAe146, and UWKA flight tracks and illustrates the type of product that was available at BOC for mission planning purposes.

Figure 6: Vertical velocities (m s^{-1}) measured by the T-REX aircraft during the coordinated three-aircraft mission on 25 Mar 2006 (IOP 6). HIAPER measurements (from 1743 to 2234 UTC) are shown in blue, BAe146 measurements (from 1720 to 1950 UTC) in red, and UWKA (from 1623 to 1853 UTC) in black. The UWKA time series, above 7 km and just below 6 km, share w-scales with the neighboring BAe146 legs. The HIAPER and BAe146 data shown is for the northern legs of their racetracks. The UWKA data within the valley is from the tracks along the south face of the box pattern, which lie in the same vertical plane as the cross-mountain tracks of this aircraft (cf. Fig. 5). The HIAPER and BAe146 tracks, which were almost perfectly aligned, were offset 3-4 km to the north from the shown UWKA tracks.

Figure 7: Time-height display of vertical velocity measurements (m s^{-1}) during a segment of IOP 6 from 25 Mar 2006 from the (a) West ISS wind profiler on the valley's alluvial slope, (b) the Center profiler (MISS), and (c) the East profiler (MAPR). Data in all three panels was smoothed using a running 10-minute and 150-m window. Areas of white are low signal strength or below the first sample height of the profiler. Vertical lines and circles highlight times discussed in the text.

Figure 8: Stereo pair of photographs of clouds over Owens Valley obtained during T-REX IOP 6 on 25 Mar 2006 at 171410 UTC by the DRI photogrammetric cameras located west of Lone Pine, CA at the south end of Owens Valley. The separation between cameras is

about 600 m. View is approximately toward NNW along Owens Valley with the Sierra Nevada to the left and Inyo Mountains to the right. Airflow is from left to right. In both photographs the cloud to the left is a cap cloud over the Sierra Nevada. Likewise, the cloud to the right is a rotor cloud. The latter is located approximately over the center of Owens Valley and underneath the first lee-wave crest, marking the top of the rotor circulation (cf. Fig. 6). The stereo 3-D effect can be achieved with an unaided eye using cross-eyed technique.

Figure 9: Hovmoller diagrams of the (a) zonal, and (b) meridional component of surface wind in Owens Valley during a two-day period of IOP 6 (20 UTC 24 Mar – 20 UTC 26 Mar 2006). The data shown is from the 10-m wind measurements by the DRI AWS network in Owens Valley. The horizontal axis of these diagrams is aligned with the northernmost cross-valley line of this network, which is comprised of 6 stations placed approximately 3 km apart (cf. Fig 2). This line is parallel to and located slightly to the north of the cross-valley transect of Fig. 1. Positive values in these diagrams represent, respectively, westerly and southerly winds. Time periods of the three UWKA flights during this IOP are marked with dashed lines.

Figure 10: (a) PPI scan of radial velocity from the DLR Doppler lidar obtained in the late afternoon hours of 25 Mar 2006 during IOP 6 (032919 UTC 26 Mar 2006). Green and blue colors indicate flow towards the lidar; yellows and reds indicate flow away from the lidar. The dashed line indicates the orientation of the RHI scan shown in (b). Grey lines in (a) indicate terrain contours, which are plotted every 200 m. The RHI scan was obtained about 4 minutes after the PPI scan (at 033434 UTC 26 Mar 2006).

Figure 11: RHI (vertical) scan of aerosol backscatter obtained by REAL during IOP 1 around 0016 UTC on 3 Mar 2006. The azimuth angle of this scan is 282 degrees. Dark (black and blue) shading represents clean air while green, yellow, and red shading represents aerosol-laden air. The white arrow directed towards the right indicates westerly flow down the east side of the Sierra slopes. This relatively clean air from the west undercuts the aerosol-laden southerly flow in Owens Valley, which has an easterly

component, indicated by a thin white arrow directed towards the left. The convergence area is visible as are the resulting circulations with aerosols transported upwards and then horizontally and downward at higher elevations (indicated by the black arrows). These circulations, inferred from the animation of RHI scans, lasted for several minutes. Range rings are drawn at 3 and 6 km.

Figure 12: Dual-Doppler synthesis of the WCR data from IOP 11 (2305-2311 UTC 9 Apr 2006) for a vertical cross-section of a cloud extending over Owens Valley. UWKA flight level is from west to east at approximately 6400 m MSL. The terrain is shown in 3-D perspective with the 2-D radar "curtain" overlay. The direction of view is approximately toward NW. Shown in color is the reflectivity factor (low values in blue/green, high values in red/magenta). Selected streamlines from the retrieved 2-D velocity field are shown in black.

Figure 13: Comparisons of wind speed and relative humidity at the 500 and 700 hPa pressure levels for IOP soundings launched simultaneously from the southern San Joaquin Valley and from Owens Valley, immediately upwind and downwind of the Sierra Nevada.

Figure 14: Energy flux (EF) versus the scalar product of mean wind vector (**U**) and momentum flux (**MF**) for six Track B HIAPER flights (from IOP 4, 6, 9, 10, and 13). Each point in this diagram represents a single flight leg in the approximate range of altitudes from 9 to 14 km.

Figure 15: Time series of (a) O_3 and CO mixing ratio, and (b) potential temperature and vertical velocity during a 7-min segment of the ferry leg of HIAPER flight on 15 Apr 2006 (IOP 13). This flight segment was over central Nevada (38.6° N and 115° W) at the altitude of approximately 14 km. The estimated HIAPER speed was ~260 m s^{-1}. The waves have horizontal wavelength of ~9 km.

Figure 16: (a) Potential temperature, wind speed, and wind direction profiles from Owens Valley rawinsonde released at 1051 UTC 30 Mar 2006 during EOP 2. Ridge top height and

wind directions forming the three-layer structure are indicated. (b) Along-valley RHI scan of radial velocity from the DLR Doppler lidar. North is to the left; green denotes flow toward the lidar, and yellow is flow away from the lidar. Note the reversing flow patterns at the elevations corresponding to the wind shifts in the top panel. Zero km lidar range corresponds to ~1 km MSL in the rawinsonde profile and vice versa. (c) Schematic illustrating the three-layer wind structure in the valley.

Table 1:

T-REX ground-based instruments, their locations, supporting institutions, dates of participation, and relevant references. OV stands for Owens Valley. For list of other acronyms, see Appendix B.

Instrument	Location	Institution	Dates	Reference
LIDARS				
Doppler Lidar (CTI Wind Tracer)	Western OV	DLR	15 Mar–25 Apr	http://www.pa.op.dlr.de/trex/
Doppler Lidar (CTI Wind Tracer)	Central OV	ASU	1 Mar – 30 Apr	none
REAL	Western OV	NCAR	1 Mar – 30 Apr	http://www.eol.ucar.edu/lidar/ Mayor and Spuler (2004) Spuler and Mayor (2005)
RADARS				
K-band radar	Sequoia National Park, Sierra Foothills	Yale	1 Mar – 30 Apr	none
WIND PROFILERS				
ISS/MAPR	Central OV	NCAR	1 Mar – 30 Apr	http://www.eol.ucar.edu/rtf/ Cohn et al. (2001)
ISS2	Western OV	NCAR	1 Mar – 30 Apr	http://www.eol.ucar.edu/rtf/ Parsons et al. (1994)
ISS/MISS	OV, Mobile	NCAR	1 Mar – 30 Apr	http://www.eol.ucar.edu/rtf/
SODARS				
Sodar/RASS	Central OV Independence Airport	NCAR	1 Mar–30 Apr	none
Sodar/RASS	Central OV – MAPR site	ASU	1 Mar – 30 Apr	none
Sodar	North OV – Big Pine	U Houston	1 Mar – 30 Apr	none
PHOTOGRAPHIC IMAGING				
Photogrammetric cameras	South OV – Line Pine	DRI	1 Mar – 30 Apr	none
Video cameras	OV, Bishop	Yale	1 Mar – 30 Apr	none

SURFACE SENSORS				
16 AWS	OV, south of Independence	DRI	long-term	http://www.wrcc.dri.edu/trex/ Grubišić and Xiao (2006)
16 AWS	OV, north of Independence	U Leeds	1 Mar – 30 Apr	none
50 temperature data loggers	OV, 2 cross- and 1 along-valley transects	U Utah	1 Mar – 30 Apr	http://www.met.utah.edu/whiteman/T_REX/
23 soil moisture sensors	OV	UC Berkeley	1 Mar – 30 Apr	none
3 ISFF	West, Central, South OV	NCAR	1 Mar – 30 Apr	http://www.eol.ucar.edu/rtf/
1 flux tower	Central OV	ASU	1 Mar – 30 Apr	none
1 flux tower	North OV – Big Pine	U Houston	1 Mar – 30 Apr	none
3 flux towers	Central OV	U Leeds	1 Mar – 30 Apr	none
OTIHS	West ISFF site	NCAR	1 Mar – 30 Apr	none
WOW	OV, Mobile	U Innsbruck	21 Mar–13 Apr	http://imgi.uibk.ac.at/mmetgroup/trex/
UPPER-AIR SOUNDING SYSTEMS				
MGAUS	San Joaquin Valley, Mobile	NCAR	1 Mar – 30 Apr	none
GPS radiosonde	Lemoore, CA	NAS Lemoore	1 Mar – 30 Apr	none
Thermosonde/Radiosonde	Three Rivers, CA Sierra Foothills	AFRL	20 Mar – 4 Apr	none
GPS radiosonde	OV, Independence Airport	U Leeds	1 Mar – 30 Apr	none

Table 2

Real-time, or near real-time, modeling systems used for mission planning during the T-REX campaign.

Model	Model Type	Organization	Horizontal Resolution	Forecast Length
COAMPS	Mesoscale nonhydrostatic	NRL	2 km	48 h Twice daily
MM5	Mesoscale nonhydrostatic	AFWA	5 km	48 h Twice daily
WRF-NMM	Mesoscale nonhydrostatic	NWS-Las Vegas	4 km	60 h Twice daily
WRF-NMM	Mesoscale nonhydrostatic	NOAA-ESRL	2 km	24 h Once daily
WRF-ARW	Mesoscale nonhydrostatic	NOAA-ESRL	2 km	24 h Once daily
WRF-ARW	Mesoscale nonhydrostatic	ARL	2 km	24 h Once daily
ECMWF IFS	Global spectral hydrostatic	ECMWF and DLR Diagnostics	~25 km	156 h Twice daily
NCEP GFS	Global spectral hydrostatic	NOAA-NCEP	~50 km	384 h Four x daily
Unified Model	Global nonhydrostatic	Met Office	~40 km	240 h Twice daily
NOGAPS	Global spectral hydrostatic	NRL	~55 km	168 h Twice daily
NRL-Yale Wave Model	Linear nonhydrostatic	NRL	2 km	36 h Twice daily
3dVOM Wave Model	Linear nonhydrostatic	Met Office UK	1 km	72 h Once daily

Table 3

IOP summary. Wind direction at approximately 4000 m obtained from soundings launched at MGAUS or NAS Lemoore sites upstream of the Sierra Nevada. Top row contains directions from the soundings launched during or prior to UWKA flights. The bottom numbers are the mean wind direction and its standard deviation for an IOP computed from all upstream soundings (SJV/SF). SJV/SF and OV stand for San Joaquin Valley/Sierra Foothills and Owens Valley, respectively. Three preset tracks and their azimuths are: A (275 deg), B (245 deg), and C (215 deg).

IOP	Date/Time	Wind Direction (deg)	Track	# of Aircraft Flights (Dropsondes)			Radiosondes	
				HIAPER	BAe146	UWKA	SJV/SF	OV
1	00 UTC 2 Mar to 15 UTC 3 Mar	240, 210 219±17	B, C	1 (17)	0	2	12	14
2	17 UTC 5 Mar to 03 UTC 7 Mar	230 214±15	C	1 (18)	0	1	10	15
3	11 UTC 9 Mar to 18 UTC 10 Mar	300, 285 303±29	A	1 (12)	0	2	11	14
4	20 UTC 13 Mar to 06 UTC 15 Mar	240, 230 254±23	B	1 (31)	0	2	12	15
5	14 UTC 20 Mar to 00 UTC 21 Mar	240 NA	B	0	0	1	2	5
6	20 UTC 24 Mar to 05 UTC 26 Mar	250,250,250 244±6	B	1 (32)	3 (20)	3	15	12
7	11 UTC 28 Mar to 17 UTC 28 Mar	250 NA	N/A	0	0	0	1	3
8	11 UTC 31 Mar to 17 UTC 01 Apr	230 243±16	B	0	1 (8)	1	12	10
9	11 UTC 02 Apr to 06 UTC 03 Apr	245, 235 234±15	B	1 (33)	2 (12)	2	13	8
10	05 UTC 08 Apr to 03 UTC 09 Apr	235, 235 235±9	B	1 (31)	2 (20)	2	6	8
11	22 UTC 09 Apr to 02 UTC 10 Apr	225 NA	B	0	0	1	1	1
12	11 UTC 11 Apr to 00 UTC 12 Apr	240 233±7	C	0	0	1	4	5
13	20 UTC 15 Apr to 08 UTC 17 Apr	260,250,250 252±7	B	2 (37)	0	3	11	14
14	08 UTC 21 Apr to 00 UTC 22 Apr	180 182±14	C	1 (21)	0	1	6	6
15	08 UTC 26 Apr to 12 UTC 27 Apr	95, 15 89±24	B (HIAPER) various (UWKA)	1 (41)	0	2	8	11

Table 4

EOP summary. Wind speed (m s^{-1}) and direction (deg) at the Sierra crest level (4418 m) at approximately 0900 UTC from Independence soundings.

EOP	Date/time	[1]Wind speed	[1]Wind direction	Special data coverage	Description
1	2300 UTC 22 Mar to 2000 UTC 23 Mar	7.3	260	BAe146 aircraft flight; REAL and DLR lidars	southerly up-valley flow
2	2300 UTC 29 Mar to 2000 UTC 30 Mar	17.0	300	BAe146 aircraft flight; REAL, ASU and DLR lidars	three-layer flow structure
3	2300 UTC 18 Apr to 2000 UTC 19 Apr	2.6	350	REAL lidar; virtual wind-towers from DLR and ASU Doppler lidars	weakest large-scale flow regime; richest observational dataset
4	2300 UTC 28 Apr to 2000 UTC 29 Apr	6.3	320	ASU lidar	nocturnal northerly down-valley flow
5	2300 UTC 29 Apr to 2000 UTC 30 Apr	1.2-4.7	Variable; NW-SW-W	ASU lidar	nocturnal northerly down-valley flow

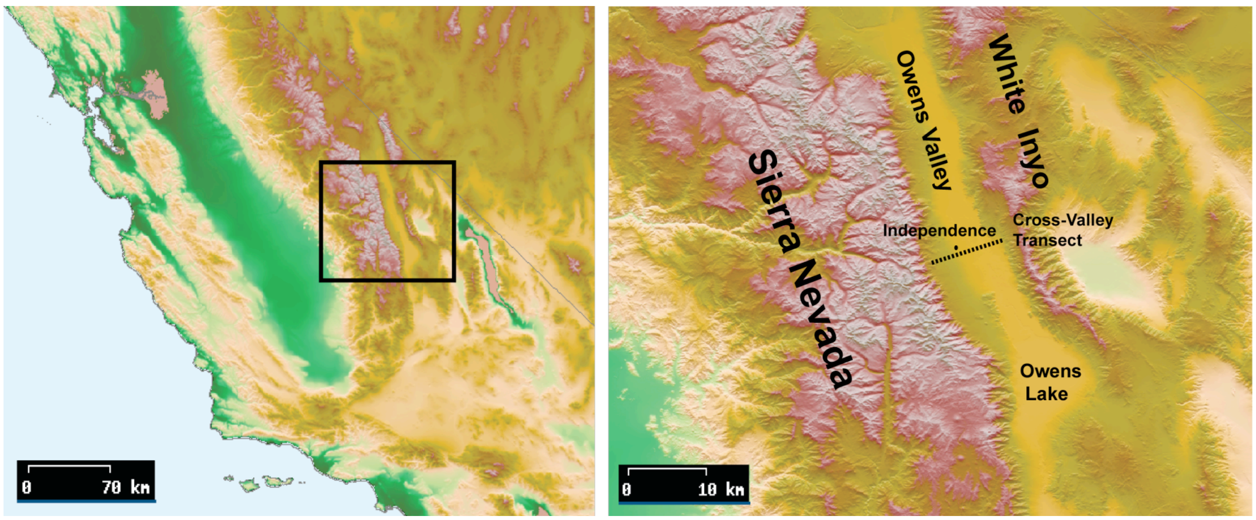

Figure 1:

Color relief map of the central and southern Sierra Nevada (left panel) and Owens Valley (right panel). The nearly north-south oriented Owens Valley lies in between the Sierra Nevada and the White-Inyo mountain ranges, which, respectively, define its west and east walls. The black dotted line in the right panel shows the cross-valley measurement transect south of Independence, California and the location of the dry bed of Owens Lake.

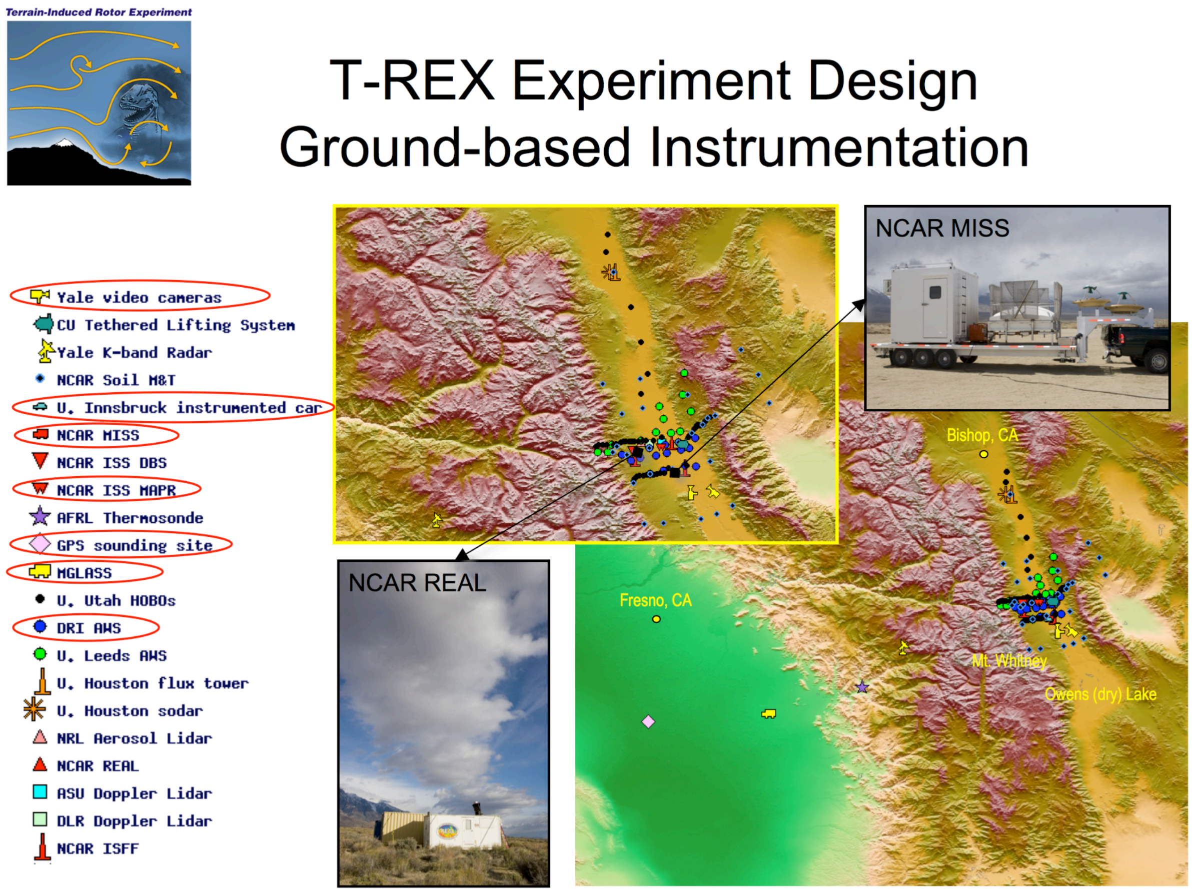

Figure 2:

Color relief map of the southern Sierra Nevada showing the T-REX field campaign area and the ground-based instrumentation. The inset map provides additional detail of the focus area within Owens Valley. The photos illustrate two NCAR systems: aerosol lidar (REAL) and mobile wind profiler (MISS). The instrumentation systems circled in the legend were deployed also in the Sierra Rotors Project in 2004. The T-REX logo is shown up in the upper left.

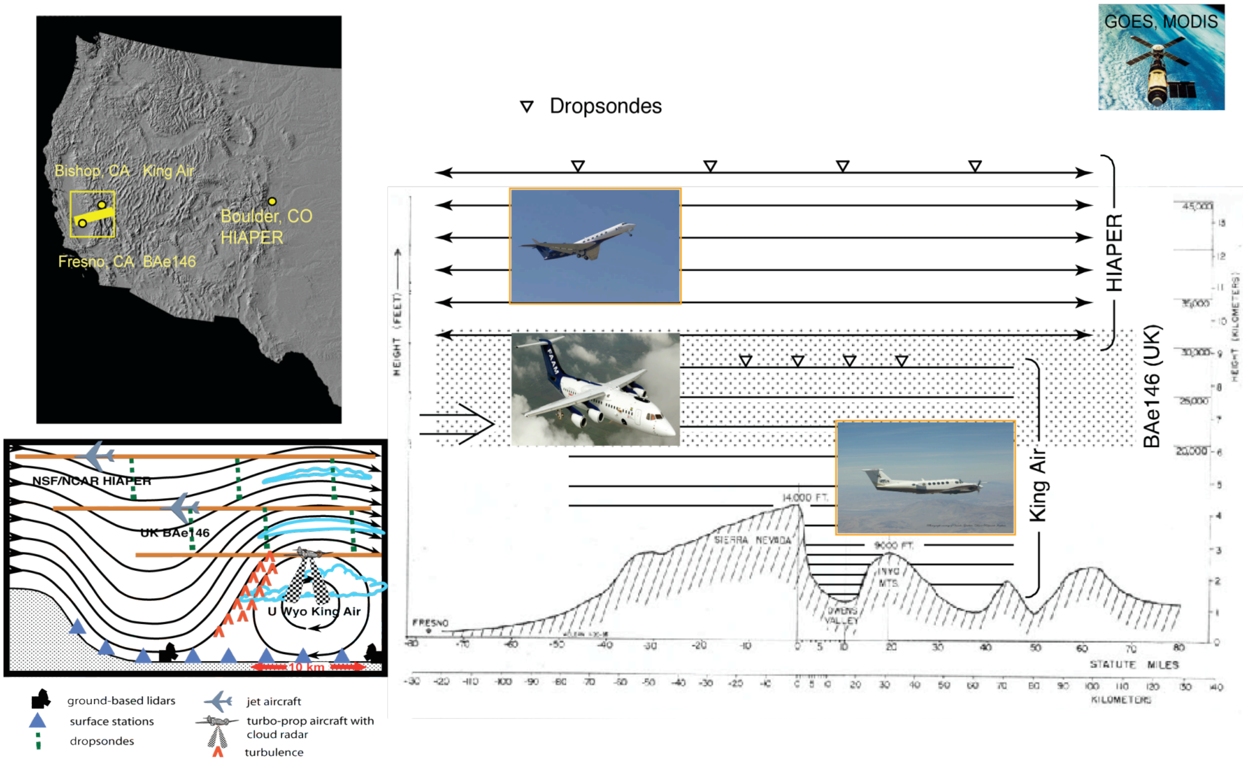

Figure 3

Composite image of the T-REX airborne platforms with the generic cross-mountain aircraft flight tracks and the vertical range of aircraft shown in relation to the terrain. The baseline of this vertical cross-section is indicated with a solid yellow line in the shaded relief map in the upper left. Yellow circles indicate the three aircraft operation bases: Boulder, CO (HIAPER); Fresno, CA (BAe146); Bishop, CA (UWKA). The schematic in the lower left shows the three aircraft flight levels in approximate relation to the rotor and lee wave and rotor clouds (based on a diagram by Ludlam and Scorer (1958)). Red carets indicate increased levels of turbulence.

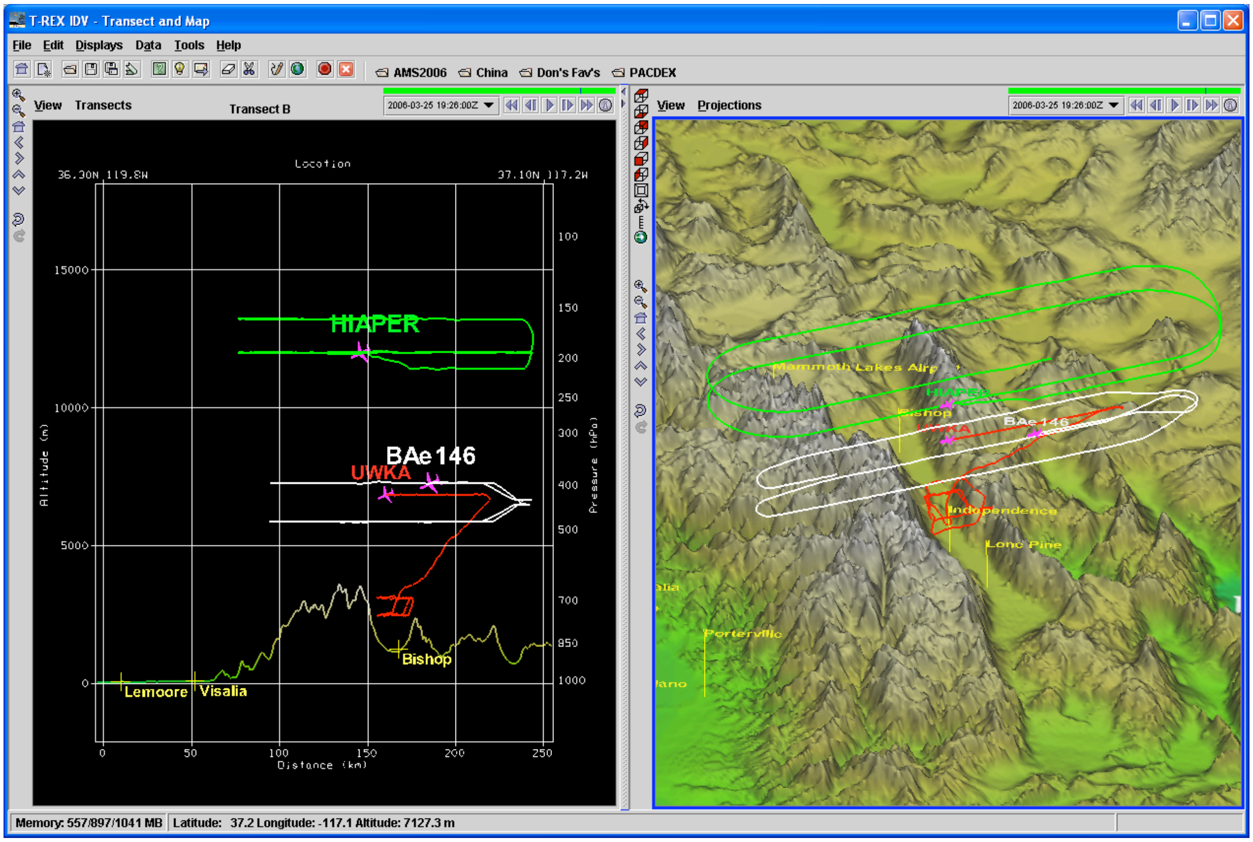

Figure 4:

Unidata Integrated Data Viewer (IDV) display of aircraft tracks in the three-aircraft coordinated mission of T-REX IOP 6 on 25 Mar 2006.

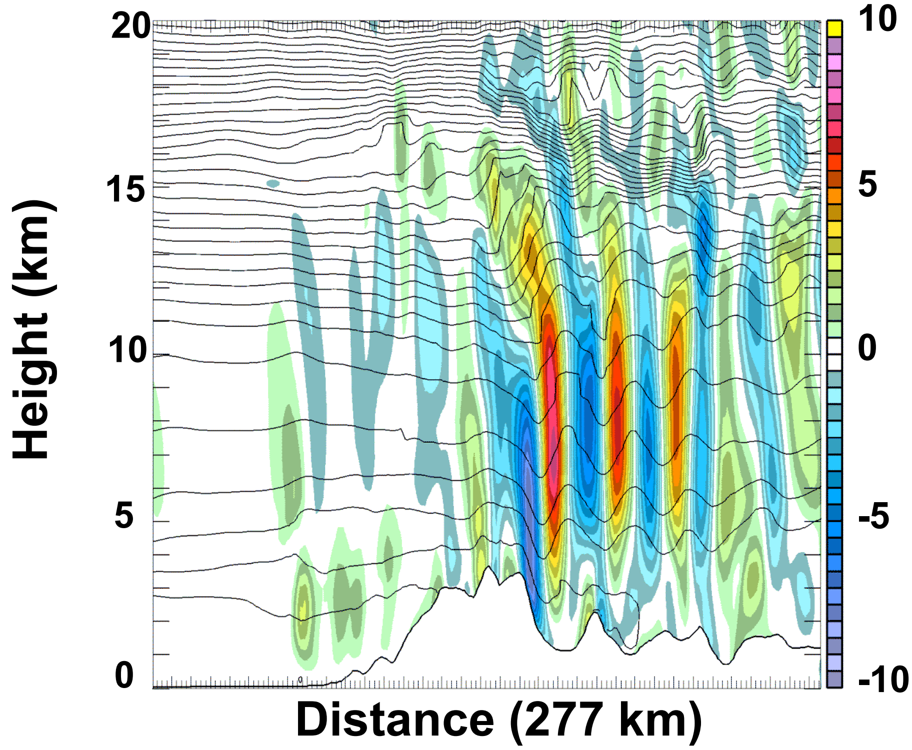

Figure 5:

Vertical velocity (color scale, increment 0.5 m s^{-1}) and potential temperature (contours interval 6 K) from a real-time 30-h COAMPS forecast for the innermost grid mesh (Δx=2 km) valid at 2100 UTC 25 Mar 2006 during IOP 6. The cross section is constructed through Independence along the HIAPER, BAe146, and UWKA flight tracks and illustrates the type of product that was available at BOC for mission planning purposes.

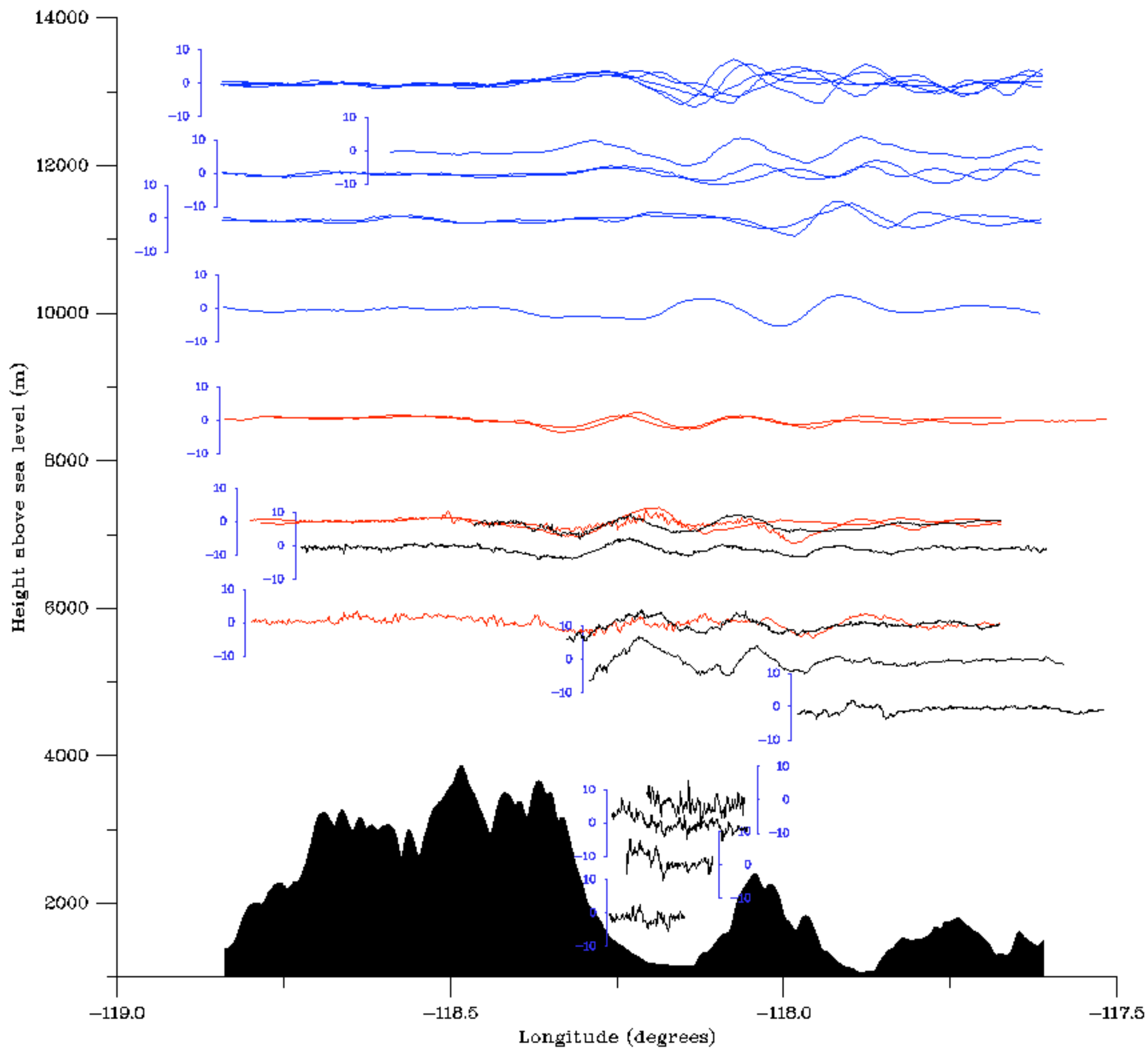

Figure 6:

Vertical velocities (m s^{-1}) measured by the T-REX aircraft during the coordinated three-aircraft mission on 25 Mar 2006 (IOP 6). HIAPER measurements (from 1743 to 2234 UTC) are shown in blue, BAe146 measurements (from 1720 to 1950 UTC) in red, and UWKA (from 1623 to 1853 UTC) in black. The UWKA time series, above 7 km and just below 6 km, share w-scales with the neighboring BAe146 legs. The HIAPER and BAe146 data shown is for the northern legs of their racetracks. The UWKA data within the valley is from the tracks along the south face of the box pattern, which lie in the same vertical plane as the cross-mountain tracks of this aircraft (cf. Fig. 5). The HIAPER and BAe146 tracks, which were almost perfectly aligned, were offset 3-4 km to the north from the shown UWKA tracks.

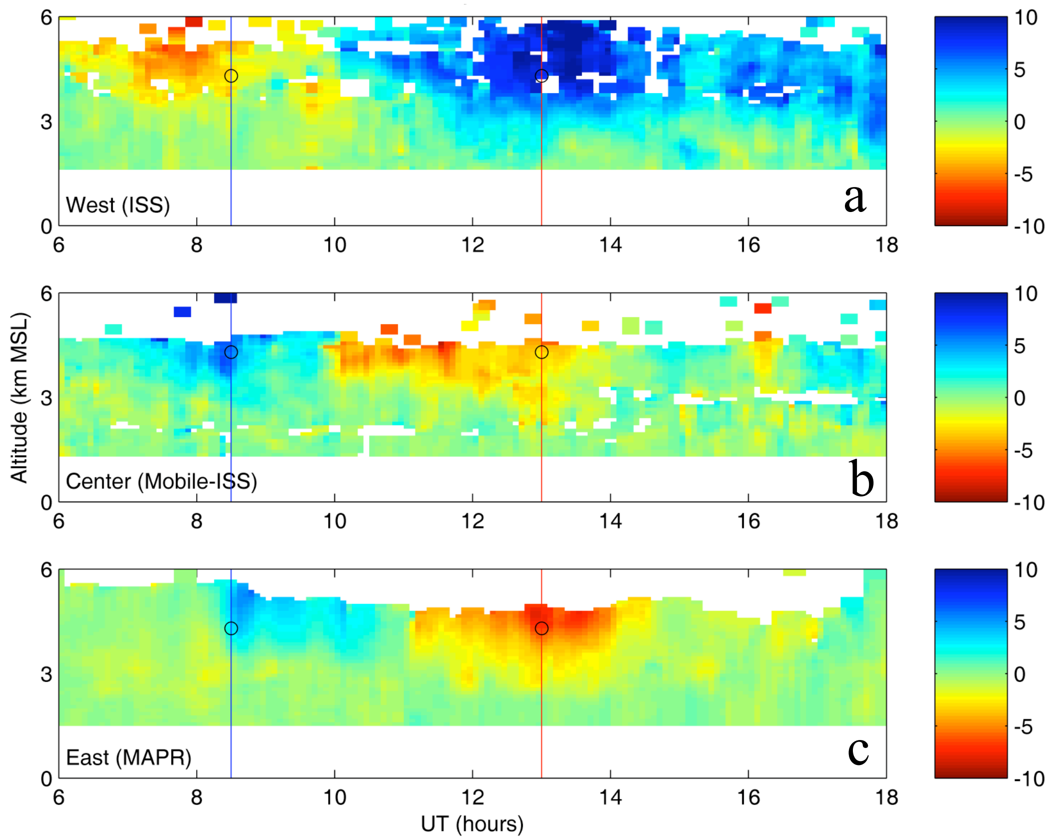

Figure 7:

Time-height display of vertical velocity measurements (m s^{-1}) during a segment of IOP 6 from 25 Mar 2006 from the (a) West ISS wind profiler on the valley's alluvial slope, (b) the Center profiler (MISS), and (c) the East profiler (MAPR). Data in all three panels was smoothed using a running 10-minute and 150-m window. Areas of white are low signal strength or below the first sample height of the profiler. Vertical lines and circles highlight times discussed in the text.

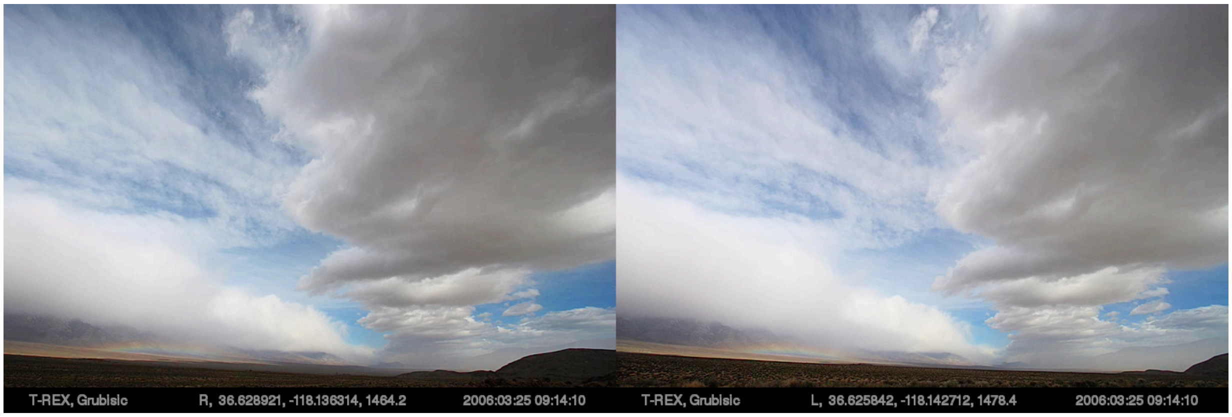

Figure 8:

Stereo pair of photographs of clouds over Owens Valley obtained during T-REX IOP 6 on 25 Mar 2006 at 171410 UTC by the DRI photogrammetric cameras located west of Lone Pine, CA at the south end of Owens Valley. The separation between cameras is about 600 m. View is approximately toward NNW along Owens Valley with the Sierra Nevada to the left and Inyo Mountains to the right. Airflow is from left to right. In both photographs the cloud to the left is a cap cloud over the Sierra Nevada. Likewise, the cloud to the right is a rotor cloud. The latter is located approximately over the center of Owens Valley and underneath the first lee-wave crest, marking the top of the rotor circulation (cf. Fig. 6). The stereo 3-D effect can be achieved with an unaided eye using cross-eyed technique.

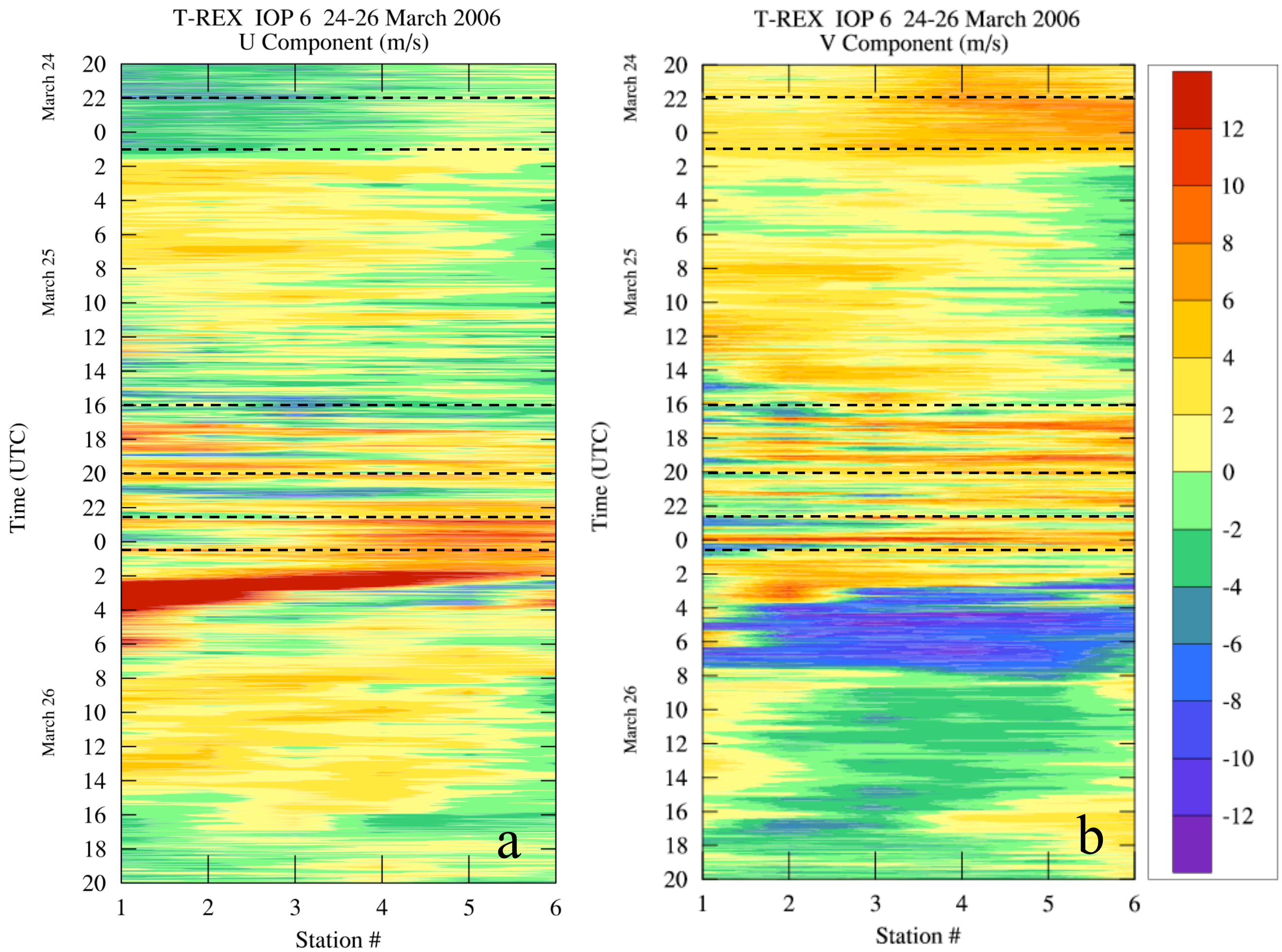

Figure 9:

Hovmoller diagrams of the (a) zonal, and (b) meridional component of surface wind in Owens Valley during a two-day period of IOP 6 (20 UTC 24 Mar – 20 UTC 26 Mar 2006). The data shown is from the 10-m wind measurements by the DRI AWS network in Owens Valley. The horizontal axis of these diagrams is aligned with the northernmost cross-valley line of this network, which is comprised of 6 stations placed approximately 3 km apart (cf. Fig 2). This line is parallel to and located slightly to the north of the cross-valley transect of Fig. 1. Positive values in these diagrams represent, respectively, westerly and southerly winds. Time periods of the three UWKA flights during this IOP are marked with dashed lines.

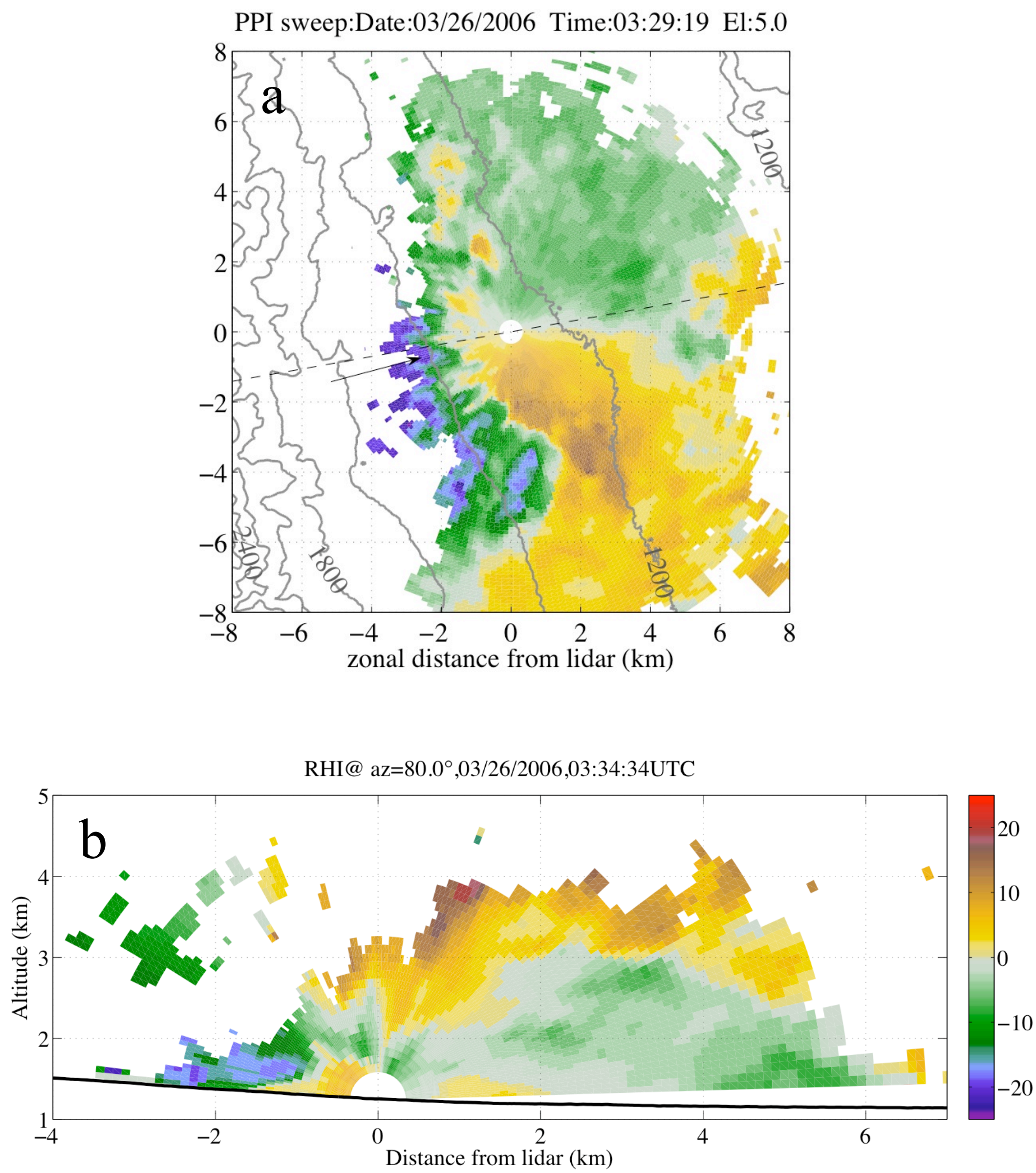

Figure 10:

(a) PPI scan of radial velocity from the DLR Doppler lidar obtained in the late afternoon hours of 25 Mar 2006 during IOP 6 (032919 UTC 26 Mar 2006). Green and blue colors indicate flow towards the lidar; yellows and reds indicate flow away from the lidar. The dashed line indicates the orientation of the RHI scan shown in (b). Grey lines in (a) indicate terrain contours, which are plotted every 200 m. The RHI scan was obtained about 4 minutes after the PPI scan (at 033434 UTC 26 Mar 2006).

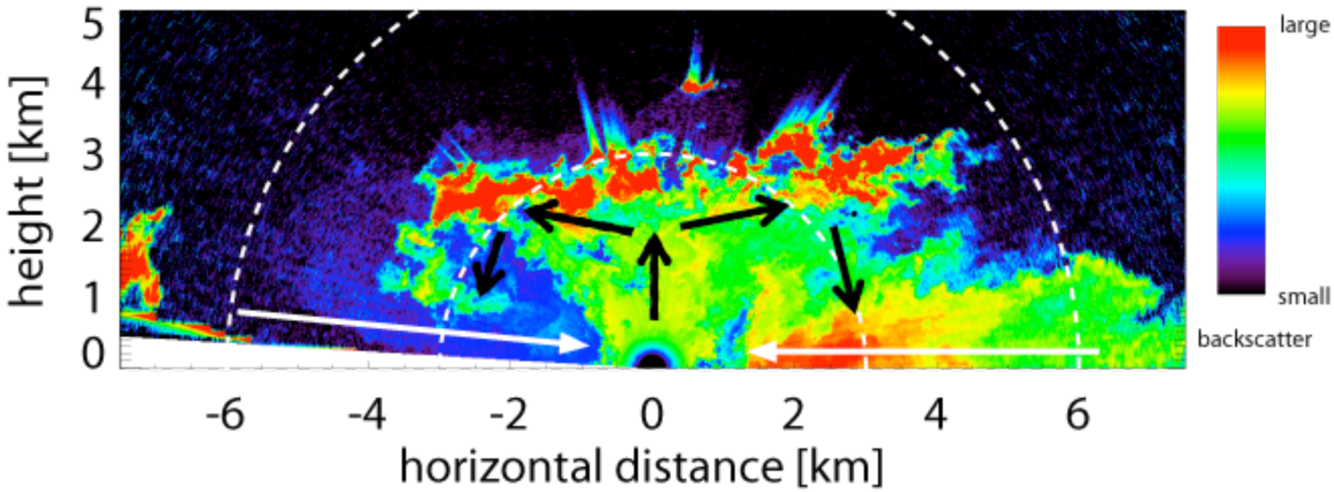

Figure 11:

RHI (vertical) scan of aerosol backscatter obtained by REAL during IOP 1 around 0016 UTC on 3 Mar 2006. The azimuth angle of this scan is 282 degrees. Dark (black and blue) shading represents clean air while green, yellow, and red shading represents aerosol-laden air. The white arrow directed towards the right indicates westerly flow down the east side of the Sierra slopes. This relatively clean air from the west undercuts the aerosol-laden southerly flow in Owens Valley, which has an easterly component, indicated by a thin white arrow directed towards the left. The convergence area is visible as are the resulting circulations with aerosols transported upwards and then horizontally and downward at higher elevations (indicated by the black arrows). These circulations, inferred from the animation of RHI scans, lasted for several minutes. Range rings are drawn at 3 and 6 km.

WCR configuration during T-REX experiment

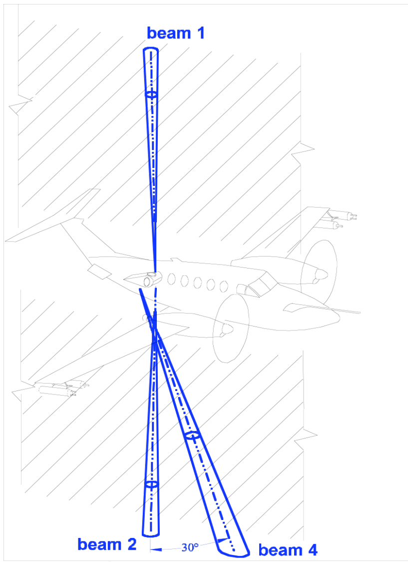

Transmit Frequency	94.92 GHz
Peak Power / Duty Cycle	1.6 KW / 1 %
Antennas: ▪ Up (beam 1) ▪ Down (beam 2) ▪ Down-fore (beam 4)	3 aperture/beamwidth/polarization 0.31 m / 0.7° / single, linear 0.46 m / 0.5° / single, linear 0.38 m / 0.6° / single, linear
Antenna utilization modes : ▪ Up+VPDD ▪ VeticalPlaneDualDoppler,VPDD ▪ Profiling Up+Down ▪ Up	Beams: 1,2,4 2,4 1,2 1
Receiver channels: ▪ receiver outputs: ▪ receiver dynamic range	2 mag: log; phase: linear > 70 dB
Dwell time/ Along-track sampling	30 ms / 3 – 5 m (typical)
Min. detectable signal (Up-antenna)	-30 dBZ @ 1km, 250ns, 500 avg
Resolution: ▪ range ▪ volume @ 1 km, 250 ns pulse	 15 – 75 m (30 m typical) 37 x 12 x 15 m
Doppler velocity processor: ▪ pulse pair	 1st & 2nd moments
Max unambiguous Doppler	±15.8 m/s

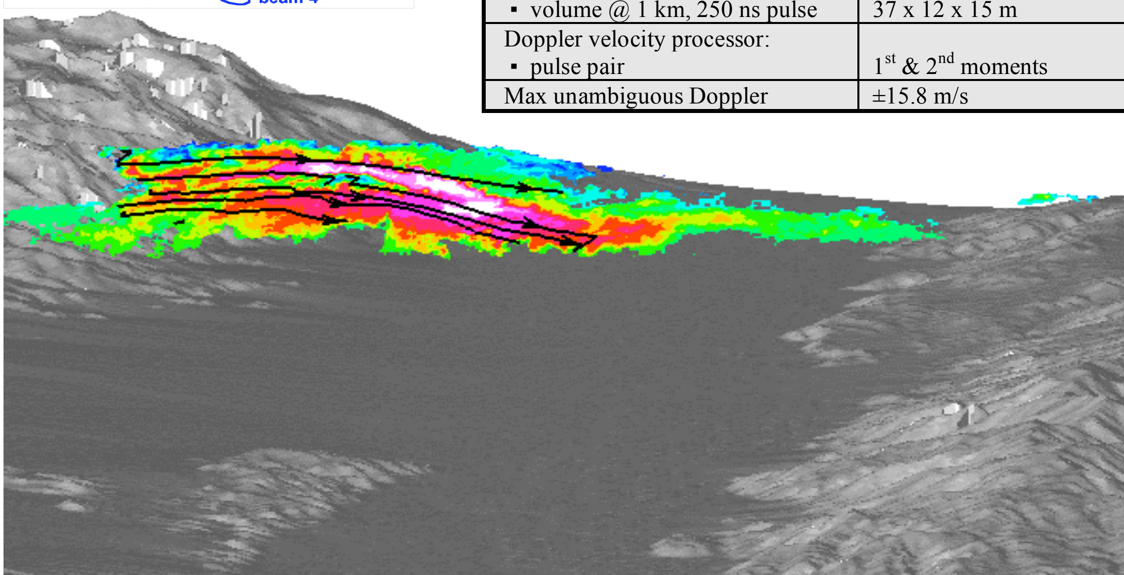

W

Figure 12:

Dual-Doppler synthesis of the WCR data from IOP 11 (2305-2311 UTC 9 Apr 2006) for a vertical cross-section of a cloud extending over Owens Valley. UWKA flight level is from west to east at approximately 6400 m MSL. The terrain is shown in 3-D perspective with the 2-D radar “curtain” overlay. The direction of view is approximately toward NW. Shown in color is the reflectivity factor (low values in blue/green, high values in red/magenta). Selected streamlines from the retrieved 2-D velocity field are shown in black.

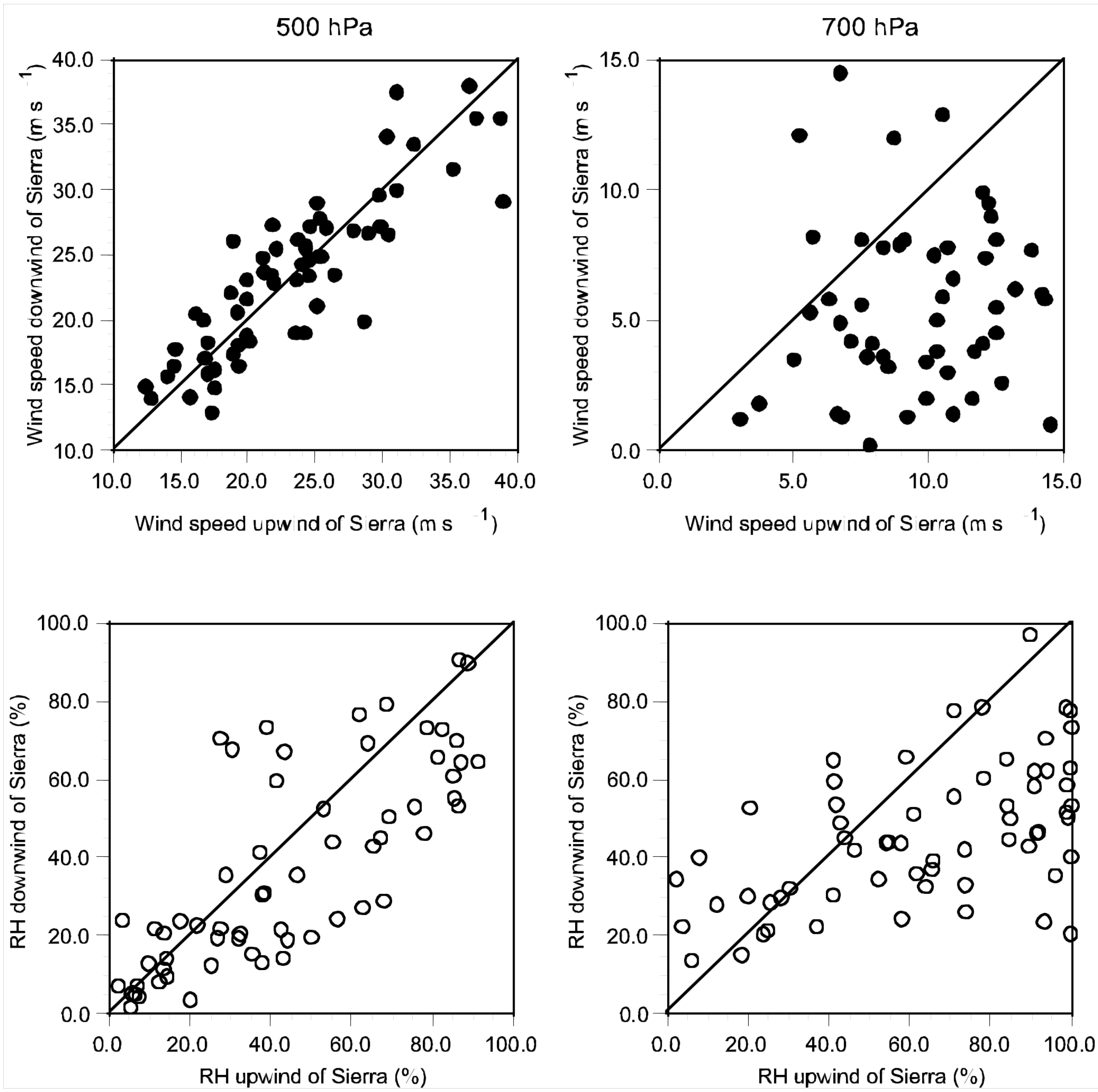

Figure 13:

Comparisons of wind speed and relative humidity at the 500 and 700 hPa pressure levels for IOP soundings launched simultaneously from the southern San Joaquin Valley and from Owens Valley, immediately upwind and downwind of the Sierra Nevada.

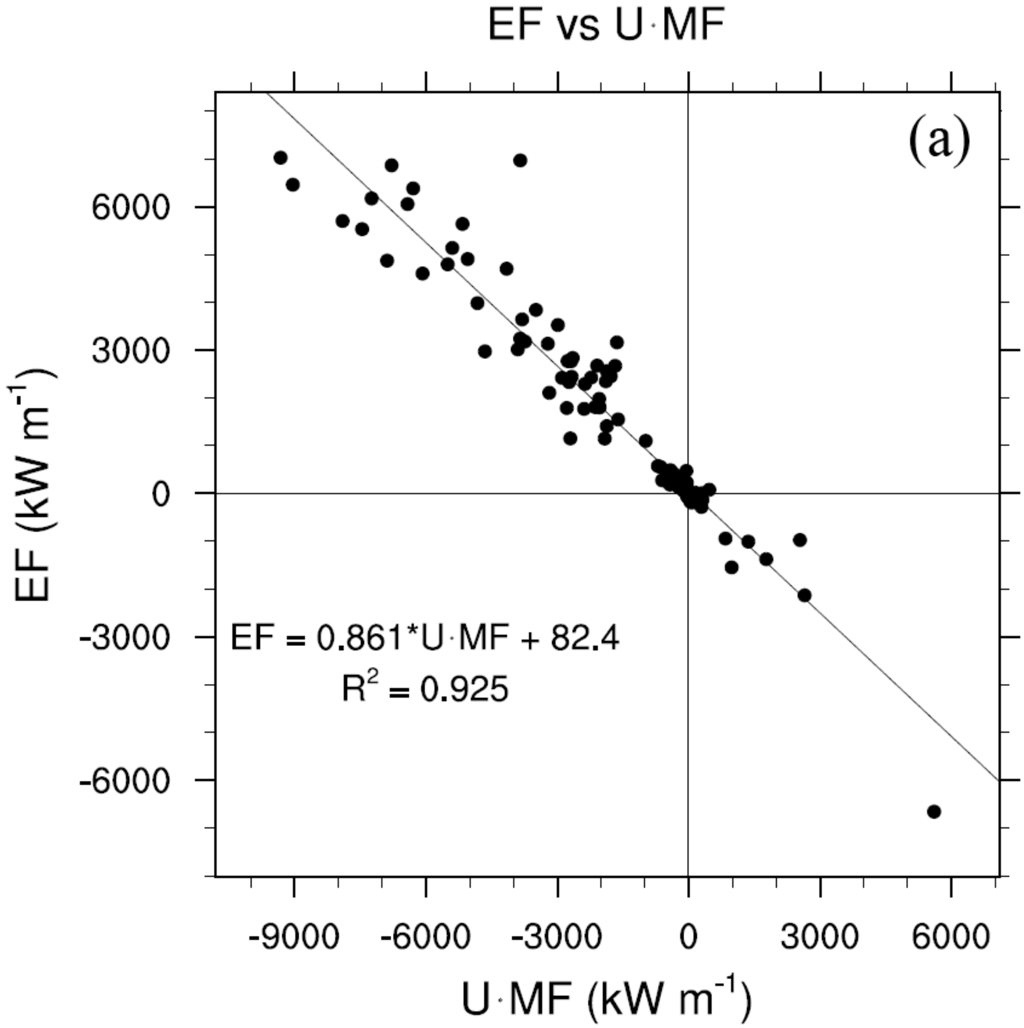

Figure 14:

Energy flux (EF) versus the scalar product of mean wind vector (**U**) and momentum flux (**MF**) for six Track B HIAPER flights (from IOP 4, 6, 9, 10, and 13). Each point in this diagram represents a single flight leg in the approximate range of altitudes from 9 to 14 km.

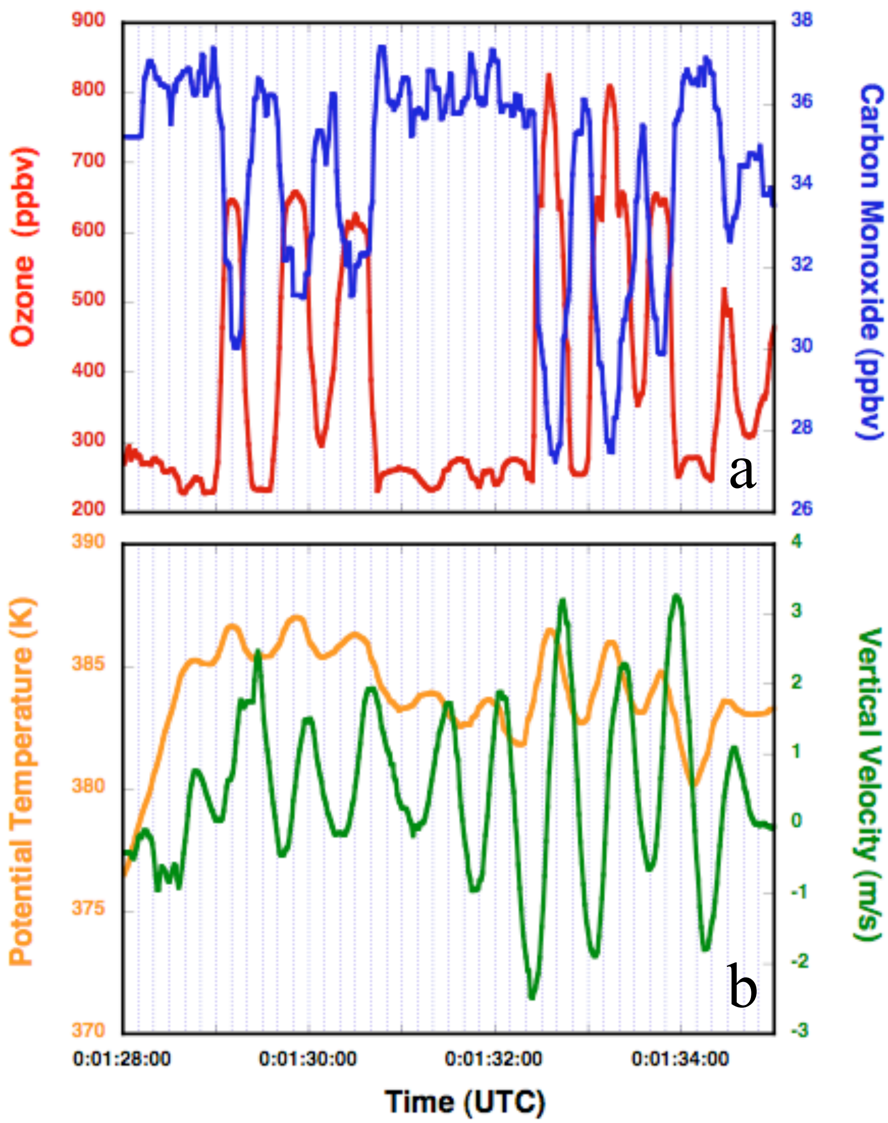

Figure 15:

Time series of (a) O_3 and CO mixing ratio, and (b) potential temperature and vertical velocity during a 7-min segment of the ferry leg of HIAPER flight on 15 Apr 2006 (IOP 13). This flight segment was over central Nevada (38.6° N and 115° W) at the altitude of approximately 14 km. The estimated HIAPER speed was ~260 m s^{-1}. The waves have horizontal wavelength of ~9 km.

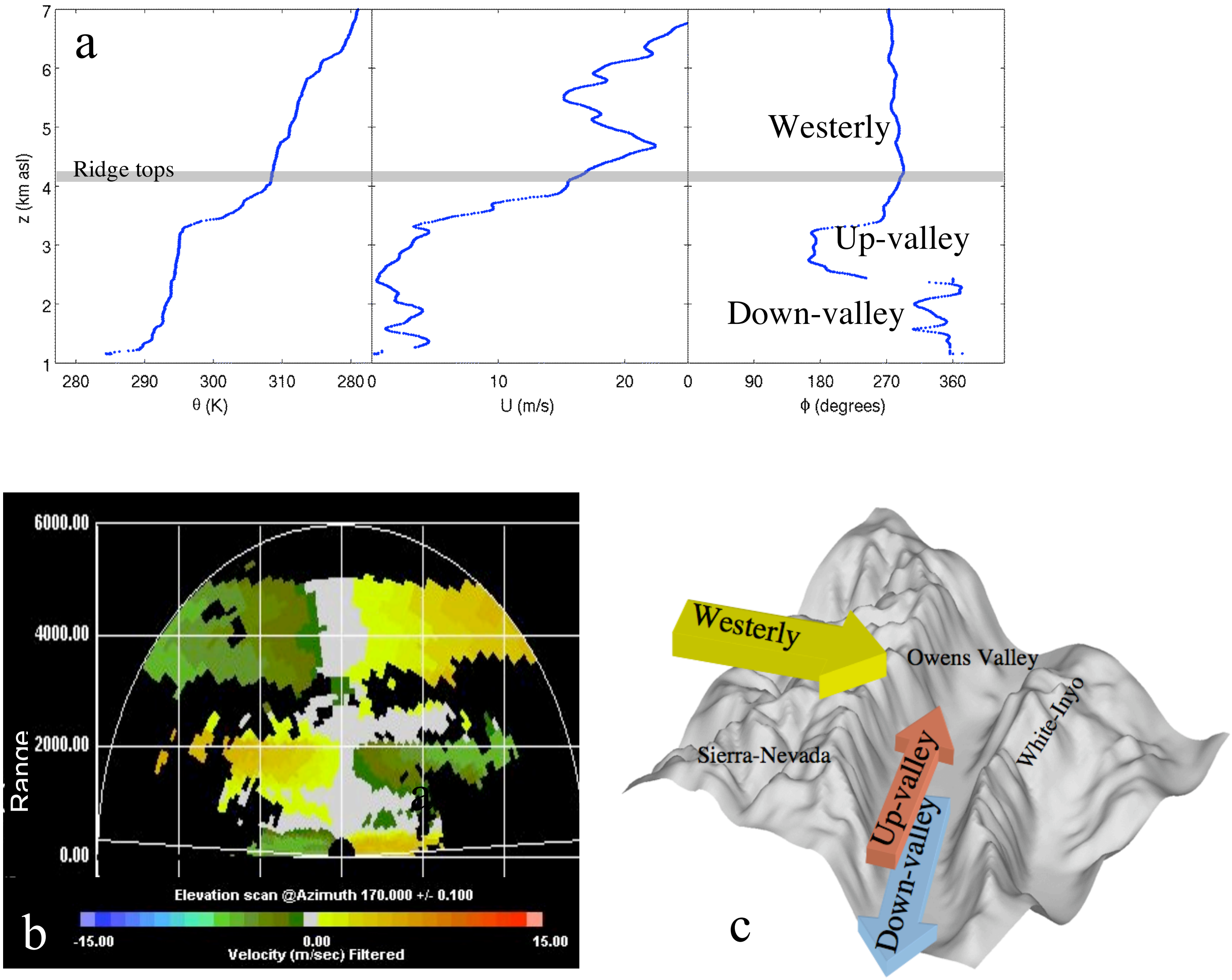

Figure 16:

(a) Potential temperature, wind speed, and wind direction profiles from Owens Valley rawinsonde released at 1051 UTC 30 Mar 2006 during EOP 2. Ridge top height and wind directions forming the three-layer structure are indicated. (b) Along-valley RHI scan of radial velocity from the DLR Doppler lidar. North is to the left; green denotes flow toward the lidar, and yellow is flow away from the lidar. Note the reversing flow patterns at the elevations corresponding to the wind shifts in the top panel. Zero km lidar range corresponds to ~1 km MSL in the rawinsonde profile and vice versa. (c) Schematic illustrating the three-layer wind structure in the valley.